Selection of High Temperature Organic Materials for Future Stirling Convertors

Euy-Sik Eugene Shin[1]
Ohio Aerospace Institute, NASA Glenn Research Center, 21000 Brookpark Rd., MS 49-1, Cleveland, OH 44135de

In the future higher temperature Stirling convertors for improved efficiency and performance, various high temperature organic materials have been demanded as essential components for their unique properties and functions such as bonding, potting, sealing, thread locking, insulation, and lubrication. The higher temperature capabilities would also allow current SOA convertors to be used in additional missions, particularly those that require a Venus fly by for a gravity assist. Stirling convertor radioisotope generators have been developed for potential future space applications including Lunar/Mars surface power or a variety of spacecraft and vehicles, especially with a long mission cycle, sometimes up to 17 years, such as deep space exploration. Thus, performance, durability, and reliability of the organics should be critically evaluated in terms of comprehensive structure-process-service environment relations based on the potential mission specifications. The initial efforts in screening the high temperature candidates focused on the most susceptible organics, such as adhesive, potting compound, o-ring, shrink tubing, and thread locker materials in conjunction with commercially available materials. More systematic and practical test methodologies that were developed and optimized based on the extensive organic evaluations and validations performed for various Stirling convertor types were employed to determine thermal stability, outgassing, and material compatibility of the selected organic candidates against their functional requirements. Processing and fabrication conditions and procedures were also optimized. This paper presents results of the three-step candidate evaluation processes, their application limitations, and the final selection recommendations.

Nomenclature

ASTM	=	American Society for Testing and Materials
ATR	=	Attenuated Total Reflectance
BS	=	British Standards
C_B	=	Compression set expressed as percentage of the original deflection
CHD	=	Cross Head Displacement
ΔH_R	=	Residual Heat of Reaction
ΔH_T	=	Total Heat of Reaction
DAQ	=	Data Acquisition
DMA	=	Dynamic Mechanical Analysis
$\Delta\sigma$	=	Static Strength - extrapolated strength from initial SN curve, psi
$\Delta Wt\%$	=	Weight change in percent
E' or G'	=	Tensile or shear storage modulus from DMA
E_Y	=	Young's modulus
E_T	=	Tangent modulus
ε	=	Strain or Elongation
ε_f	=	Strain-to-failure or Ultimate Elongation
EN	=	European Standards
FT-IR	=	Fourier transform- infrared spectroscopy
FS	=	Fatigue Strength

[1] Principal Scientist, Research Team Manager-Materials, Ohio Aerospace Institute (OAI).

GC/TCD = Gas Chromatography/Thermal Conductivity Detector
HT = High Temperature
ID = Inner Diameter
IR = Infradred
mDSC = Modulated Differential Scanning Calorimetry
Mw = Molecular Weight
OD = Outer Diameter
sOM = Stereo Optical Microscopy
PET = Polyethylene terephthalate
PV = Pressure vessel
RGA = Residual Gas Analysis
RT = Room temperature
RVDT = Rotary Variable Differential Transformer
SDLT = Synergistic Durability Life Testing
SN = Stress-Number of Cycle at Failure
SOA = State-of-the-Art
SOP = Standardized Operating Procedure
ST = Shrink Tubing
σ_f = Tensile strength
t = Time
T = Temperature or Bondline thickness of lap shear specimen
T_β = Sub T_g transition temperature
T_d = Thermal degradation on-set temperature
T_{end} = Endothermic peak temperature
T_{exo} = Exothermic peak temperature
T_g = Glass transition temperature
T_m = Melting temperature
T_{max} = Maximum temperature
T_r = Relaxation temperature
T_t = Transition temperature
TCIOP = Temperature-alone Combined In-situ Outgassing with Pre-mix gas
TGA = Thermo-Gravimetric Analysis
TL = Thread Locker
TMA = Thermo-Mechanical Analyzer
UHP = Ultra high purity, 99.999w%

I. Introduction

DEVELOPMENT of the Stirling radioisotope generator has been a key part of recent NASA's Radioisotope Power Systems (RPS) Program mailinly due to its high fuel efficiency[1-2]. For the latest SOA advanced generator designed and manufactured under the joint sponsorship of the Department of Energy (DOE) and NASA, Lockheed Martin Corporation of Valley Forge, NASA Glenn Research Center (GRC), and Sunpower Inc[3-5], reliability and durability of every components and materials used in the convertor have been extensively and systematically evaluated for a potential flight hardware development, subsequently the organic materials used were successfully validated for such convertor application. Even though the flight project was terminated prematually due to budget constraints, the overall successful performance demonstrations of the system encouraged NASA to continue the development of Stirling RPS technology, especially for higher temperature amd more efficient convertors.

Due to their inherent susceptibility to temperature and radiation as well as less predictable time-dependency on their properties and performance, a new class of organic materials has to be selected for upcoming high temperature convertors, particularly focusing on thermal stability, durability, radiation hardness, outgassing behavior, and synergistic effects of vaious combined in-service conditions. Typically, thermal stability and durability of the organics were assessed by accelerated thermal aging experiments at a few elevated temperatures in conjunction with longer-term life testing. The rate of aging processes was normally accelerated by temperature, thus temperature was often used as an accelerator for the accelerated aging test to predict longer term thermal stability of the organics. However, it could be only valid when the degradation mechanisms were not altered within the test temperature

range. Systematic and practical test methodologies developed and optimized based on the extensive organic evaluations and validations performed for various Stirling convertor types for more than a decade[6-10] were employed to determine thermal stability, radiation hardness, outgassing, and material compatibility of the selected organic candidates in terms of their functional requirements while their process and fabrication conditions and procedures were also being optimized. Figure 1 shows the overall program plan employed in selecting the best high temperature organic candidates with the optimized test methodologies. For the four most susceptible organics, the plan was completed up to the final candidate selection, but the SDLT step was postponed due to re-planning of the overall Stirling technology development research at GRC. The test results and key findings to date are discussed in the sequence of the program steps for every organic material types.

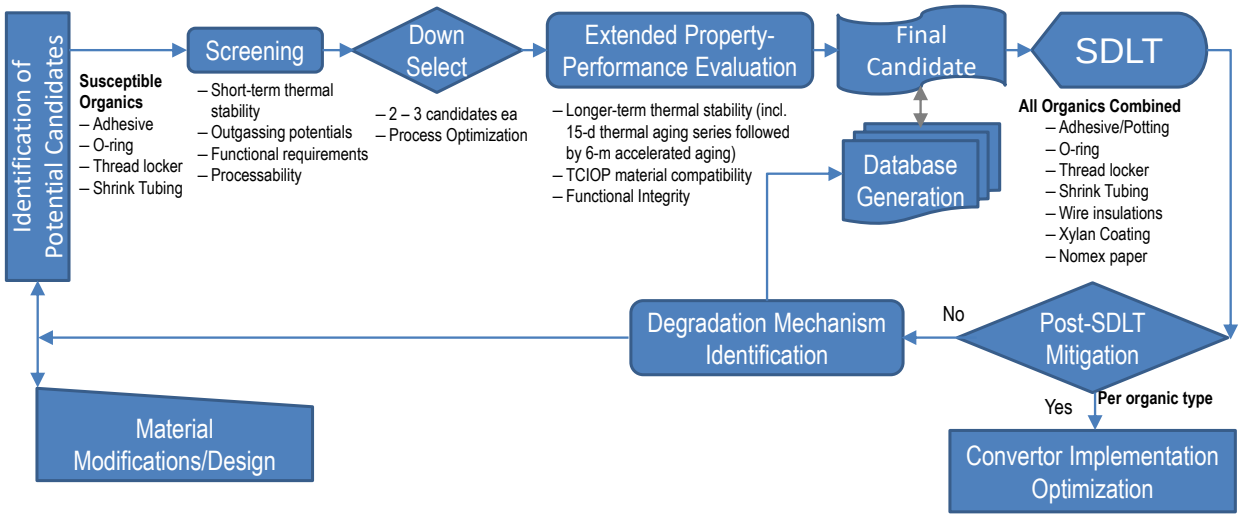

Figure 1. Overall program plan to down-select high temperature organic materials.

II. Materials and Processes

The initial efforts in screening the high temperature candidates focused on the most susceptible organics, such as adhesive, potting compound, o-ring, shrink tubing, and thread locker. Initially targeting long-term use at ~ 165 °C or higher, several potential candidates per organic material type were identified from commercially available products that were mostly based on the manufacturer's data sheet or recommendations, in terms of maximum use temperature, processing/installation temperature, and processability. All materials investigated are summarized in Table 1.

Table 1. List of commercial candidates identified for each organic material type.

Organic type	Material	Brand	Maker	Max. T, °C	Install T, °C	Product properties
Adhesive/ Potting	Epoxy	Hysol EA9394C-2	Henkel	232	93/115	Two part epoxy paste filled with aluminum particle; long pot-life (8 hours at 25 °C)
	Cyanate ester	FM2555	Cytec	232	177/227	Supported film adhesive on structural carrier; 0.06 psf film
	Cyanate ester	RS-4A	YLA		177	Unsupported film adhesive; 0.03 psf film
	Epoxy	L-313U	JD Lincoln	204	135/213	Unsupported film adhesive; 0.05 psf film
	Epoxy	AF191K AF191U	3M	204	177/204	Supported (0.08 psf) or unsupported (0.055 psf) film adhesive
	Epoxy	AF131-2	3M	232	177	Flexible scrim supported film adhesive, 0.075 psf

Thread Locker	Dimethacrylate ester	Loctite 266	Henkel	232	25 – 40	One part, surface insensitive, high strength, high temperature anaerobic thread locking material
	Dimethacrylate ester	Loctite 294	Henkel	204	25 – 40	One part, low viscosity, high temperature anaerobic thread locking and sealing material
	Epoxy	Resbond 507TS	Cotronics	260	25	Two parts epoxy-based thread locker and sealant but filled with PTFE particle for lubricity
	Ceramic	Resbond 907TS	Cotronics	1148	25/121	Water-based proprietary material, cured by moisture removal
	Polyethylene terephthalate	Poly-Lok Patch	Long-Lok Fasteners	204	25	Solidified plastic locker patched on fasteners at predetermined locations with optimum amount
Shrink tubing	Polyimide	208X	Dunstone	220–400	350	Shrink ratio > 1.12:1; highest temperature shrinkable film commercially available
	PEEK	PEEK	ZEUS	260	330	Shrink ratio > 1.4:1; excellent abrasion resistance and radiation resistance
	Teflon copolymer	PFA	ZEUS	260	340	Shrink ratio > 1.4:1; improved thermal stability and radiation resistance
	ETFE	RT-555	Raychem	200	220	Shrink ratio > 2:1; extremely resistant to hydrocarbons, low outgassing
	Silicone	SRFR	Raychem	200	175	Shrink ratio > 1.5:1; extremely flexible
O-ring	Silicone	70SLR	Marco	200	n/a	Baseline material for current SOA convertors
		S1151	Marco	315	n/a	High temperature formulation
	Perfluoro-elastomer/Fluorocarbon Rubber (FFKM)	Kalrez	DuPont	260	n/a	Excellent chemical and temperature resistance
		Markez Z1028	Marco	300	n/a	Black, excellent chemical compatibility and high temperature capabilities
		Markez Z1307	Marco	275	n/a	Translucent; semi-crystalline nano-filled; low out-gassing; high temp capabilities

Adhesive/potting candidates were either processed in a hot press or autoclave after conventional vacuum-bagging. The standard cure conditions initially employed were based on manufacturer's recommendations. The two part Hysol EA9394C-2 epoxy was mixed in a Thinky mixer (ARE-250, THINKY CORP) using the following conditions: 1 min hand mixing; 3 min defoaming at 2200 rpm; 3 min mixing at 2000 rpm for ~6 gram total in 12 mL jar, which was the optimum mixing condition determined for the regular EA9394 epoxy previously in terms of void content, thermal properties, and bonding performance. For adhesive/potting materials, various sheet samples were fabricated in a hot-press with the standard or optimized cure/postcure conditions, typically including a thick (~ 1.5 mm), a thin (~0.1 mm), or the thin sample but laminated between metal substrate, to mimic the potting or bonding application. The laminated thin film specimens were fabricated by vacuum-bagging and autoclave cure. However, for the AF131-2 epoxy which was only available in the scrim supported film adhesive form, the neat resin was squeezed out from a 20-ply stack of the film adhesive first at 90 – 100 °C. The neat resin was then degassed at 100 °C under 28 inHg vacuum and molded to the sheet samples for more controlled characterizations and meaningful comparisons between both candidates without interferences, such as weight or thermal property changes from the scrim material. The sheet samples were typically used for most physical-thermal property measurements, but for mechanical properties, more sophisticated test specimens were designed.

The optimum cure conditions of the TL candidates were determined during their initial screening evaluations and down-selection. It should be noted that the Loctite 266 and 294 from Henkel were a one-part anaerobic cure system in which cure initiates by contact with metallic ions when confined in the absence of air between close fitting metal surfaces. Other materials were either thermally cured or cured by moisture removal or patched thermoplastic.

Shrink tubing materials were received in expanded form but were tested in fully recovered or shrunken form. Typical test samples were 3/16" OD – 1.12" (30 mm) long sections and shrunk snugly without metal core. A loose fit was recommended by manufacturers using the optimized conditions determined during their initial screening evaluations and down-selection.

All o-ring samples were tested as purchased. The type of o-ring used was AS568-013; Nominal, 7/16" ID - 9/16" OD – 1/16" CS (Actual, 0.426" ID - 0.070" CS).

III. Experimental

A. Material Property Testing

Extensive material properties and behavior of the organics were systematically monitored not only for comparison among the candidates, but also to identify the degree of degradation and mechanisms involved in various thermal aging experiments. Most properties were identified by their performance or functional requirements of the organic materials, and were categorized by (i) physical properties involving changes in weight, dimension, color or microstructures; (ii) thermal properties; (iii) molecular/chemical structural properties; and (iv) mechanical properties.

Typical thermal properties monitored were T_m, T_g, T_β, T_r, T_t,T_{end}, T_{exo}, and ΔH by mDSC or DMA; storage modulus and loss modulus as a function of temperature by DMA; T_d by TGA and various weight loss characteristics, such as Δwt% occuring from RT to 100°C normally due to evaporation of water, from 100°C to 200°C which is typically associated with thermally-induced outgassing, or from RT to 700 °C representing char yield. Other outgassing characteristics observed by isothermal TGA analyses included Δwt% during the temperature ramp, Δwt% during the 7 hour dwell, and weight loss rate calculated at the last 100 minutes of the test. The weight loss and outgassing characteristics were presented in terms of a normalized weight by the outgas-able phase, typically Δwt% at 700°C from that of a normal TGA scan for more practical and meaningful comparison. These outgassing characteristics from various organic materials were then directly compared to their ASTM outgassing database for acceptability in the Stirling convertor applications. TGA and mDSC were typically run under dry nitrogen at a heating rate 5 °C/min and 10 °C/min, respectively, while DMA was run under air at 5 °C/min heating rate. In the case of the adhesives, the degree of cure or % cure was calculated by the residual ΔH of their exothermic peak based on the ΔH_T.

In most cases, FT-IR in ATR mode was used to assess the changes in molecular structure. For the specimens with controlled thicknesses, the IR spectra were quantified via intensities of the peaks. In the case of the TL materials, a non-contact IR scanning method via reflection mode (Nicolet NEXUS 670 with Thermo Nicolet Continuum microscope) was employed on the fasteners that were removed from the torque specimen assembly after torque testing since ATR mode was not suitable. The non-contact IR scanning via reflection mode had a zooming capacity up to ~200×. Semi-quantitative assessment of thermal degradation and molecular structural changes were monitored mostly via IR peak shape and location analyses.

Mechanical tests of various candidate materials were designed based on their functional requirements. In the case of the adhesives, bonding performance was measured in either pure shear and/or FWT mode. Custom-designed test specimens in either component-level full-cale or subscale sandwich lap shear configurations were employed for both static and fatigue loading modes[6,8,11]. The bondline between the magnet material and titanium substrate in both test specimens was designed to mimic the actual magnet bonding in the magnet-can assembly in one of the current SOA Stirling convertors. All test specimens were fabricated via vacuum-bagging and autoclave cure followed by the optimized cure and postcure cycles without further bake-out. Most mechanical testing was performed at GRC except the component-level full-scale testing which was conducted at CTL Inc. (Cincinnati, OH). For the subscale lap shear specimens, a screw-driven Instron test frame was used for all static mode testing, while two table top fatigue testers (ElectroForce model 3200 from BOSE or currently TA Instruments) equipped with a hot/cold chamber were used for all fatigue testing. The fatigue tests were conducted isothermally at 175 °C, under sinusoidal loading at 100 to 200 Hz frequency with the minimum load of 10 N. The target for the maximum number of cycles to stop the test without failure was at about 50 to 100 million cycles based on some preliminary trial experiments. More accurate measurements of the overlap area of each lap shear specimen was made from imaging the fracture surface using sOM. Figure 2 shows a typical SN curve of the adhesive bonding developed by the

subscale lap shear specimens with various properties and data analysis protocols. The residual static bond strength was determined from the samples that were fatigued and terminated at 175 °C to quantify the potential fatigue-induced degradation of bonding integrity.

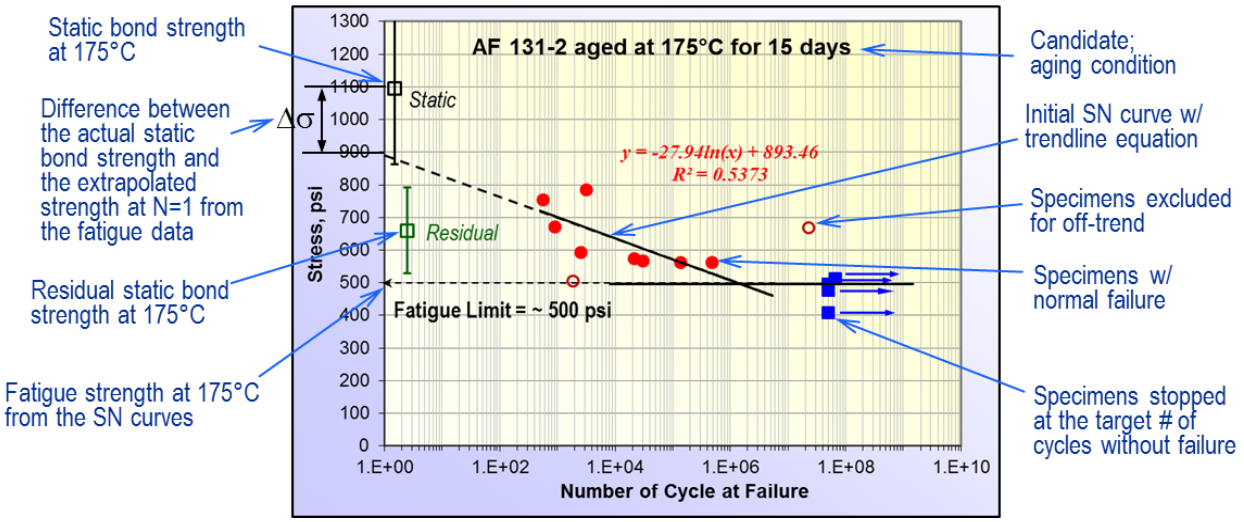

Figure 2. Typical fatigue SN curve developed for adhesive bonding using subscale lap shear specimens with standardized interpretation of a data set.

In the case of TL materials, torque strength was the main mechanical property monitored. Since there were many different types of joints involved in a typical Stirling convertor, efforts were made to determine torque strengths in a few representative joint systems, such as the magnet-can to piston in a blind hole configuration, displacer spring to spring standoff in thru-hole configuration, and flex rod to spring end or to displacer end in thru-hole configuration, as a function of temperature. After torque testing, microscopic failure mode and IR spectroscopy chemical analyses were conducted to determine changes in the molecular structure or thermal degradation with respect to the aging time and temperature. Design of the torque specimen assemblies is illustrated in Figure 3. The mating parts and washers were made of the same materials and followed the same dimensions and configurations as the actual convertor components assembled with the fasteners. The actual fasteners fabricated for a SOA convertor were used in this study. Detailed step-by-step installation procedure was developed based on the standard procedure implemented by a convertor manufacturer including the actual installation torques.

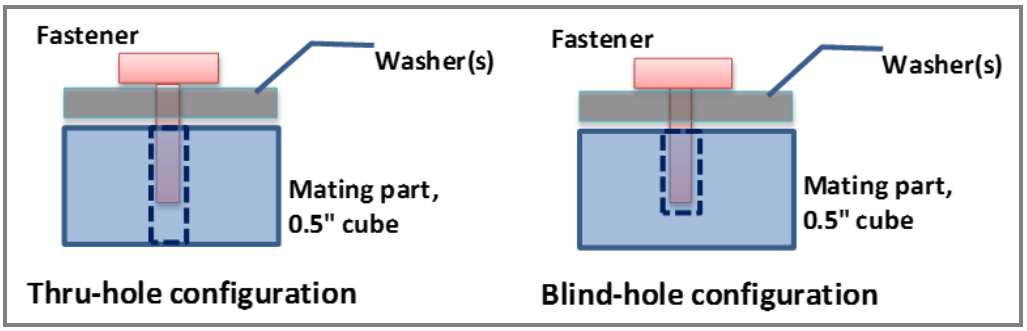

Figure 3. Schematic diagrams of torque specimen assemblies per hole configuration.

Torque strength testing was conducted on the test setup built on the table-top MTS torsion test frame (Model 858, A/T #4) consisting of high resolution torque load cell (280 N-cm capacity with ±0.5 N-cm resolution), axial tension/compression load cell, custom designed sample holder fixtures for various fastener types, and custom designed air-circulated oven rated to 300 °C. The overall setup complied the BS EN 15865 Standard. Outputs from all transducers including torque cell, axial load cell, and RVDT or angular displacement device were digitally read and stored into the designated computer hard drive by MTS Flex Test SE controller and DAQ system.

Mechanical performance of shrink tubing material was evaluated by tensile testing of a single edge notched strips specimens. Shrink tube samples were sectioned into test strips using a specially designed cutting fixture to control

specimen width accurately (~ 0.12 inch or 3 mm), axially and radially. A notched was made on one edge up to ~0.04 inch (1 mm) deep using a sharp surgical blade after mounting on another fixture that could maintain the un-notched width of the strip samples constant. The notch dimensions were measured via stereo OM and the sample thickness was measured using a caliper. A table-top MTS load frame equipped with a custom-made air-circulated oven was used for the notched tensile testing at RT and elevated temperatures. Test conditions were standardized as follows: initial grip-to-grip distance of ~ 30 mm for the axial specimen, and ~ 10 mm for the radial specimen, CHD speed of 0.5 in/min. Typically 8 repeats were run per test condition.

In the case of o-ring materials, three different mechanical tests including compression-set, hardness, and tensile test were performed followed by the ASTM standards, D395, Method B, D2240, Shore A scale, and D1414, Method B, respectively. For compression-set tests, all o-ring samples were placed between polished tool steel plates at 25% compression of original o-ring thickness and were then conditioned at 200 °C (392 °F) for 70 hours under dry N_2 gas flow in a Blue M Nitrogen oven. Hardness was measured using a Type M Durometer. Tensile tests were conducted in a screw-driven Instron test frame using a custom-designed fixture. All tests were conducted at the crosshead speed of 20 in/min. For various mechanical property testing, o-ring thickness was measured with a Randall & Stickney thickness gage using ~4 oz weight.

B. Thermal Aging

All thermal aging tests were conducted under an inert gas environment with dry shop nitrogen gas. Various ovens with either their own capability of flowing N_2 gas or employing a pressure vessel equipped with N_2 gas flow control system were set up for various aging tests. In most cases, the aging temperature and N_2 gas flow rate were monitored and adjusted daily for the entire aging intervals, and documented for future reference. All aging tests followed the standardized operating procedure (SOP)[6,9,11]. In the case of the short-term 15-day thermal aging tests involving more than seven or eight temperatures, the experiment was performed in two phases – the initial phase at four different temperatures, and then the second phase in which temperatures were determined based on the first test results to confirm the trends, and thus to ascertain more accurate temperature dependency. Since the maximum temperatures for the accelerated aging test identified for each organic type were fairly close, with the exception of the TL, it was decided to run the 6-month accelerated aging tests by combining those three organic candidates: adhesives, shrink tubing, and o-ring specimens to preserve resources. Sample boats made of stainless steel wire and sheet were used to organize and sort out various test specimens for three aging temperatures and four aging durations (i.e., four boats per aging temperature).

C. TCIOP Testing

Based on previous experiences with respect to the accurate and reliable gas analysis in terms of composition and concentration down to 10 ppm range, an integrated RGA-GC/TCD-FTIR gas analysis system directly connected to the sample PVs was developed[11]. The set-up was designed not only to combine those three analyzers into one system, but also to minimize potential sources of contamination and be capable of controlling gas temperatures. The set-up was also designed to simultaneously run two samples per experiment. In this test, various organic candidate materials were loaded into the PV and charged with the pre-mixed gases (107 ppm H_2, 1,060 ppm O_2, 3,081 ppm N_2, 312 ppm CO_2, and the balance of UHP helium) that were representative of a typical gas sample from a Stirling convertor following exposure to long-term simulation test runsup to several thousand hours.

For adhesive/potting materials, both epoxy-alone thick sample (~0.5" L x 1.0" W x ~ 0.06" t), 7 - 8 ea per epoxy type, and subscale lap shear specimens, 7 ea per epoxy type, were used. In the case of the TL material, only Loctite 294 and Resbond 507TS candidates were tested with modified torque specimen assemblies in the shape of a 0.18" inner radius, 0.5" high hexagonal prism instead of the regular 0.5" cube geometry due to the inlet size of the PV. Fifteen samples used per test for Joint type #2 and #8, in addition to a few fasteners containing thread locker residues from the 15-d thermal aging test. Then, the 0.5" cube adapter with center hexagonal hole was used for torque testing. For the shrink tubing material, 3/16" OD – 9" long sections were tested in as-received, expanded condition. Note that specimens used for the 6-month thermal aging experiment were pre-shrunk or fully recovered. The o-ring material was used in as-received form.

The standardized test procedures for TCIOP testing included the following: Specimens were preconditioned in a sealed PV. Each PV contained only one material type) → Specimens were baked-out under vacuum @ 90 °C for 24 hrs → vessels were pressurized w/ the pre-mix gas to ~ 400 psi at RT → PVs were monitored for leaks for 24 hrs → Initiated the TCIOP test. The following thermal exposure profiles were used: Temperature ramp from RT → 100 °C @ 1 °C/min with 3 day dwell → Temperature ramp to 150 °C @ 1 °C/min with 2 day dwell→ Temperature ramp to 200 °C @ 1 °C/min with 7 day dwell. A standardized outgas monitoring scheme was also developed. At t = 0 at RT (20 °C), RGA, GC-TCD, and FT-IR were all run as the baseline. During temperature ramps, only FT-IR

spectroscopy was run, one spectrum was collected every ~ 20 minutes (all gas lines were vacuumed between runs). During dwell times, RGA, GC/TCD, and FT-IR tests were run daily. For FT-IR analysis, the amount of gas sample was maintained at 1 atm pressure. In all cases, the peak intensities can be quantitatively analyzed as the actual concentration of each gas species.

After the in-situ outgassing test, the systematic residual property evaluations were conducted on the TCIOP tested samples to determine outgas-induced degradation following the aforementioned specific test methods per organic material type, whenever applicable.

IV. Results and Discussions

A. Initial Screening and Down-selection

Screening for two or three better candidates from the potential candidates was carried out by assessing their processability, short-term thermal stability, outgassing potentials, and required basic functional properties. The first three assessments were normally achieved by basic process analysis, various thermal property analyses using DSC/mDSC, TGA, isothermal TGA, and DMA, and FT-IR molecular structure analysis. The functional property/performance assessment involved (i) full-scale bond strength in both shear and normal mode as a function of temperature up to 200 °C for the adhesives, (ii) torque strength on M10 steel nuts and bolts at room temperature as a function of cure conditions for the TL, (iii) notched tensile properties in both axial and radial directions as a function of temperature up to 200 °C for the shrink tubing materials, and (iv) 200 °C compression-set and tensile properties as a function of temperature up to 200 °C for the o-rings.

Table 2 shows the typical results of preliminary screening evaluations in terms of performance ratings on each properties of adhisve/potting candidates. Based on that, both Hysol EA9394C-2 and AF131-2, were down-selected. More specifically, the 3M AF131-2 was credited for superior thermal performance and stability in terms of bond strength and high T_d, while the Hysol EA9394C-2 was considered for the best paste form adhesive due to its usefulness for multi-applications, such as bonding, laminating, and potting etc. Large supportive database from the basic formulation, EA9394, evaluated and validated for lower temperature use in a SOA Stirling convertor with long positive history in terms of processability, performance, durability and reliability was another strength of the EA9394C-2 adhesive.

Similarly, the better candidates down-selected for other organic material types were Loctite 294 and Resbond 507TS for the TL; SRFR and ETFE for the shrink tubing, and S1151 and Markez Z1028 for the o-ring. In the case of the TL, Poly-Lok PET was also selected as an alternative because of its potential to be used as a solid patch system, even though it was not experimentally evaluated. During the initial screening, the most optimum shrinking process conditions were determined for each shrink tubing candidate which included determining shrinking characteristics such as maximum shrinking ratio and directionality.

Table 2. Overall ratings of adhesive/potting candidates for down-selection.

Material type / Properties	L-313	RS-4A	FM2555	AF131-2	AF191K	EA9394C-2
Cure Condition	–	–	–	–	–	+
Processability/Applicability	0	–	–	0	0	+
Multi-purpose Application	+	–	–	–	–	+
Thermal Degradation Temperature/TGA	+	+	+	+	+	+
Weight loss/outgssing potential	–			+	0	0
Thermal Transisiton/mDSC	0	0	0	0	0	0
Shear Bond Strength	+	–	–	+	+	+
FWT Bond Strength	–			+		+
Final Selection				✓		✓
Note: 0, neutral or insignificant effect; +, positive performance; -, negative performance						

B. Extended Property-Performance Evaluations

The down-selected candidates were then further evaluated more extensively and systematically for functionality performance, longer-term thermal stability, and material compatibility for the high temperature Stirling convertor

applications, and thus for final selection of the best candidate. Processing or installation conditions of the candidates had been optimized prior to the extensive evaluations.

1. Functional Performance

Since the adhesive material was identified as the most critical organic material for the Stirling convertor application due to its single point failure reliability assessment, e.g., magnet bonding[6,8], more efforts were made especially on its functionality-related performance evaluations. It is also well known that overall performance of thermoset polymer adhesives is greatly affected by how they are cured, primarily bonding integrity, particularly under fatigue loading mode. Therefore, additional efforts were made to optimize the cure conditions of the down-selected adhesive candidates and ultimately, their fatigue performance in the full-scale component level testing.

Based on extensive evaluations in terms of cure temperature-time-% cure-thermal properties relations including the results from both 15-day thermal aging and 6-month accelerated thermal aging tests, the most acceptable optimum cure-postcure conditions, typically the degree of cure higher than 99.5% were determined for both candidates while the conditions that were not acceptable due to either under-cured state or potential thermal degradation were also identified. The optimum conditions typically required higher cure tempertures or much longer cure time than the manufacturer's recommended conditions. For example, increasing the postcure temperature to 190 – 205 °C for up to 360 hours improved thermal stability of both candidates.

From the combined cure kinetics data, a distinctive % cure-T_g correlation which can be used for performance predictions was derived for both epoxy candidates regardless of specimen thickness, Figure 4. The cure-postcure conditions caused possible thermal degradation were clearly off the trends and illustrated that their T_g was significantly lowered from those of the fully cured good samples. As can be seen in the plot, AF131-2 reached the full-cure state faster compared to the T_g increase, while EA9394C-2 showed a non-linear relationship with increasing degrees of cure. The highest T_g achieved was fairly close for both adhesive candidates, 260 °C for EA9394C-2 vs. 270 °C for AF131-2, even though the AF131-2 started with considerably higher T_g at the primary cure states. Similarly, a % cure-T_d correlation was also derived from the combined cure kinetics data for both epoxy candidates. The AF131-2 reached the full-cure state quicker than EA9394C-2 against the T_d increase even though the maximum T_d achieved in EA9394C-2 was slightly higher than that of AF131-2. The cure-thermal aging-% cure–thermal property relationship can be used to differentiate cure advancement from thermal degradation, thus to predict aging performance or thermal stability of the epoxy candidates.

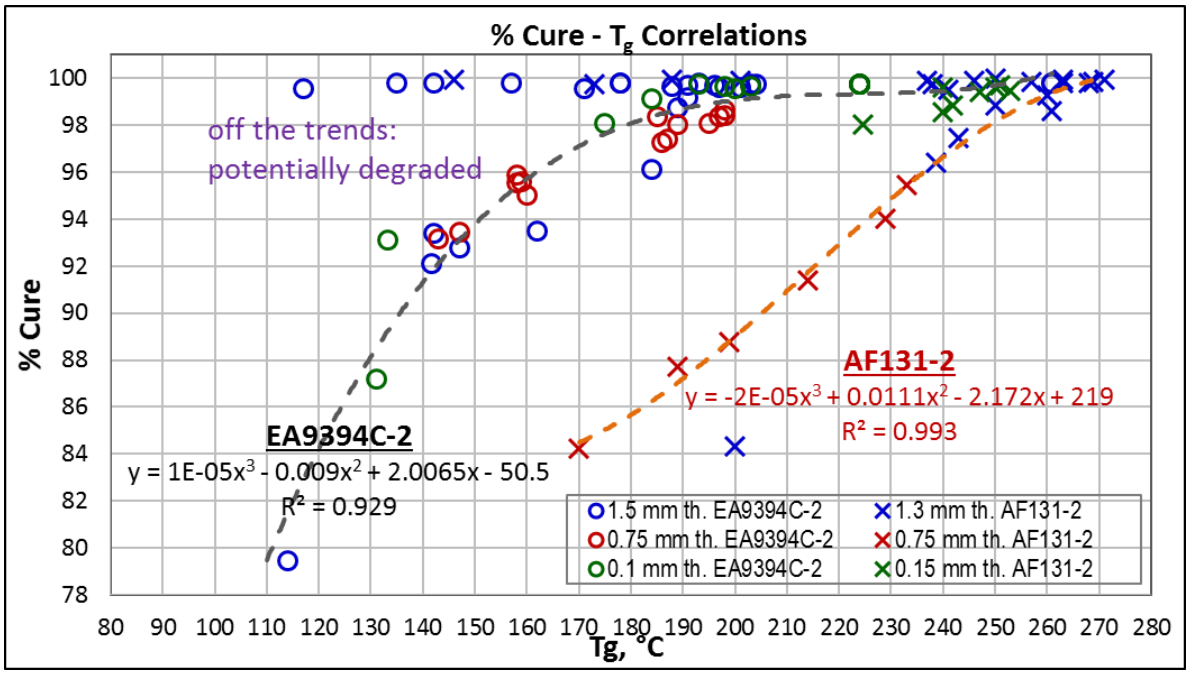

Figure 4. Degree of cure – T_g correlations of the down-selected adhesive/potting candidates.

Based on various thermal properties, degrees of cure, and outgassing characteristics as a function of cure conditions, the initial standardized cure conditions determined by the manufacturer's recommendations were

acceptable for both magnet bonding and stator potting and were thereby used for the extended performance evaluations for both adhesive candidates.

Fatigue performance of bonding between magnets to titanium magnet-can with the down-selected adhesive candidates was assessed by full-scale component level coupon testing. Figure 5 shows the master fatigue SN curves of magnet bonding at 180 °C for EA9394C-2 and AF131-2, respectively. Fatigue performance of the EA9394C-2 at 180 °C (FS=~630 psi, R=0.86) was comparable to those of the regular Hysol EA9394 tested at 115 °C (~ 800 psi, 0.74) which was evaluated extensively for the one of the current SOA Stirling convertors[6,8], but it exhibited potential to improve with further bonding process optimizations. Fatigue performance of the AF131-2 (FS=~3,500 psi, 0.97) was superior to EA9394C-2 epoxies. The results of the AF131-2 was less reliable due to a fewer data points, but the results were verified with the sub-scale sand-witch lap-shear samples as a part of thermal stability assessment. In either case, the fatigue endurance strengths of both candidates estimated from the SN curves were much higher than the theoretical bond strength needed for this application[6,8].

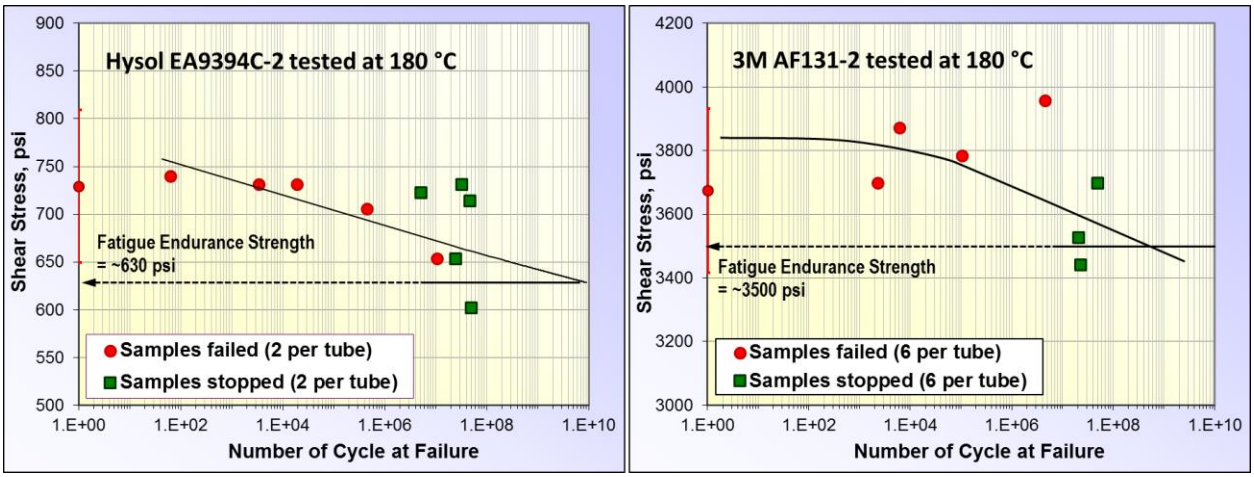

Figure 5. Fatigue SN curves of magent bonding by the down-selcted adhesive candidates at 180 °C.

2. Long-term Thermal Stability

The longer-term performance and thermal stability were evaluated by 15-day thermal aging tests at various temperatures up to 260 °C, followed by the 6-month accelerated thermal aging experiment. Typically, 2 – 3 temperatures were planned for the accelerated thermal aging tests in order to assess longer-term performance and life predictions. The maximum temperatures for the accelerated aging tests which would maintain the same aging mechanisms as the target use-temperature but accelerate their aging processes were determined from the results of the 15-day thermal aging tests.

The 15-day thermal aging experiment for the adhesive/potting candidates was completed in two test sets, the first set at four temperatures; 130, 160, 190, and 260 °C, followed by the second set at three additional temperatures at 175, 205, and 220°C. The temperatures for the second set were decided based on the results of the first set to ascertain the trends of the systematic physical, thermal, chemical, and mechanical properties from the first set. From both thin and thick epoxy alone sheet samples, the most visible changes in both color and physical appearance occurred at 260 °C where both candidates darkened significantly, and appeared to have blistered and cracked, which are signs of thermal degradation. Figure 6 illustrates that both candidates showed a dramatic change in weight loss rate around 220 – 230 °C regardless of specimen thickness, which was a strong indication of changes in aging mechanism or onset of thermal degradation. The EA9394C-2 epoxy showed slightly higher weight losses than AF131-2 epoxy in the lower aging temperature range below the transition, but considerably lower than the regular EA9394[6,8]. Its transition temperature was about 30 °C higher than the regular EA9394 epoxy.

Effects of aging temperature on static bonding performance of the candidates evaluated by the sub-scale sandwich lap shear specimens at the 120, 170, and 200 °C test temperatures are summarized in Figure 7. Both bond strength and toughness began to decrease at aging temperatures exceeding 130 °C and continued to increase as the aging temperature increased, independently of the test temperature. The rate of decrease was considerably higher after about 220 °C for both candidates. This was another indication of changes in aging mechanism or onset of thermal degradation. Slight increases in bonding properties up to 130 °C in both candidates were probably due to cure advancement during aging. Differences in bonding properties between the two candidates were narrowed with increasing aging temperature. The EA9394C-2 showed much improved bonding properties than the regular EA9394

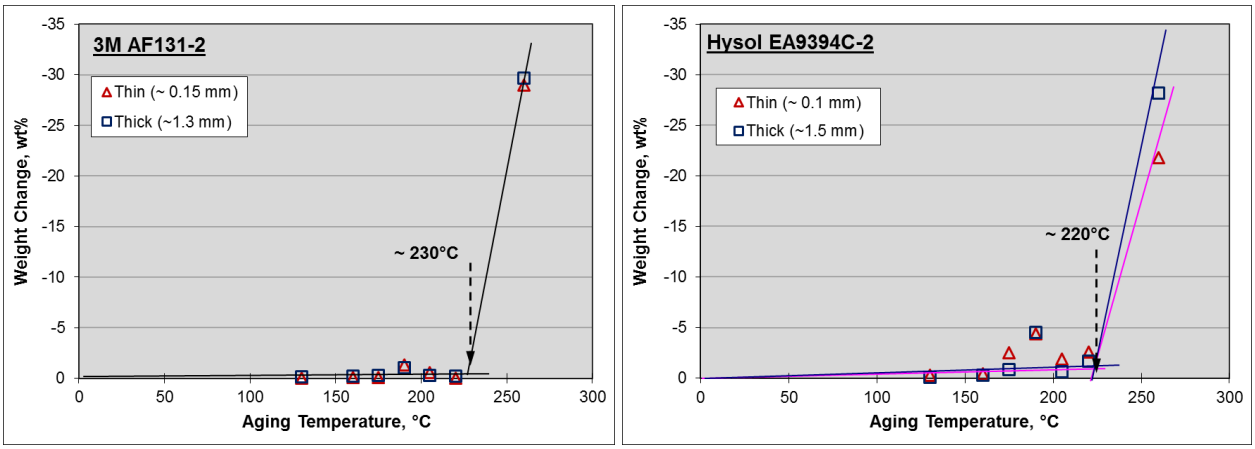

Figure 6. Weight losses of adhesive candidates after 15-day thermal aging as a function of aging temperature.

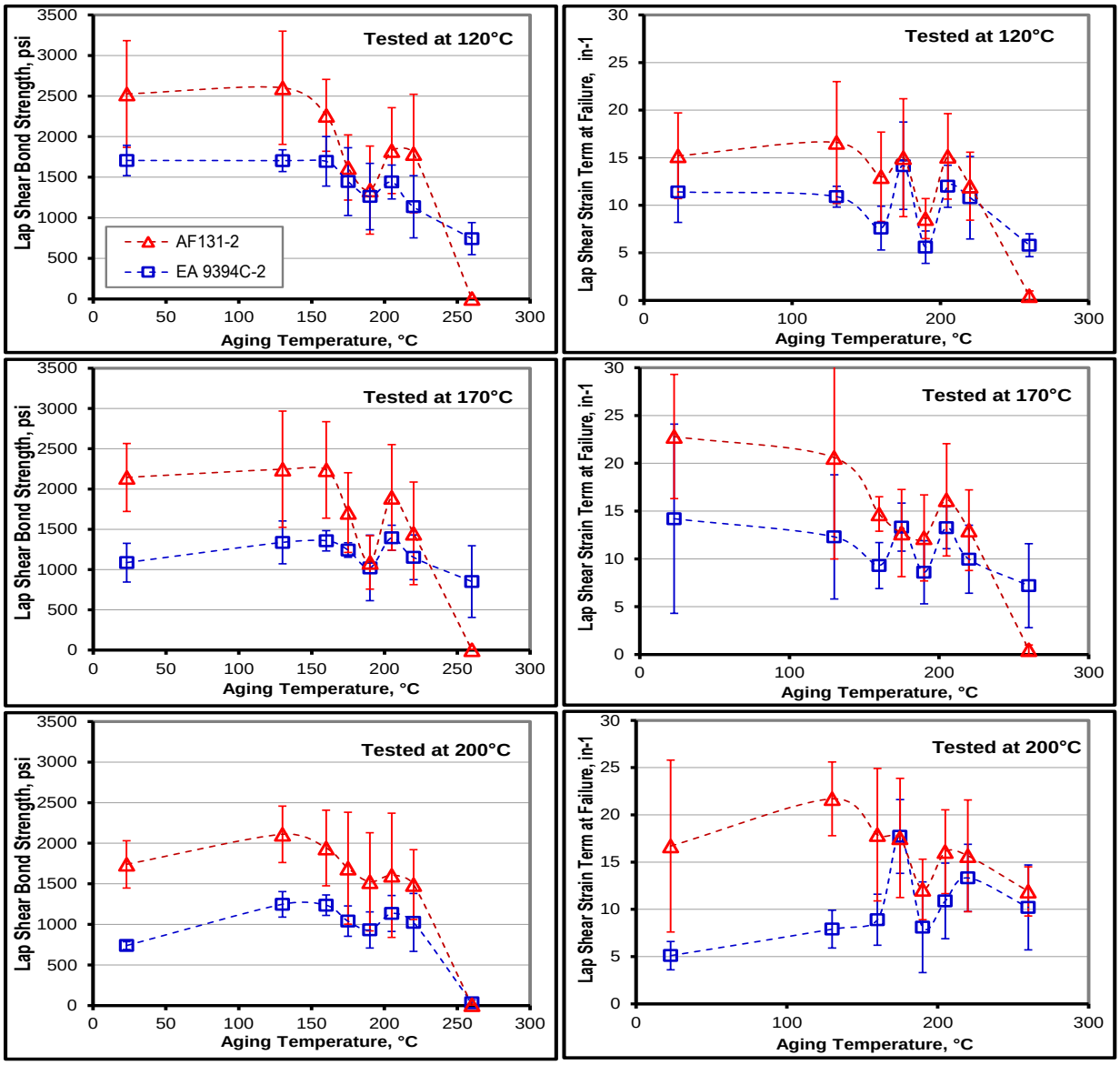

Figure 7. Lap shear bonding properties of adhesive candidates at various test temperatures as a function of 15-day thermal aging temperature.

and increased the transition temperature by ~ 30°C. A similar transition was observed from other thermal properties including T_g, T_d, and Δwt at 700 °C at around 220 – 230 °C regardless of sample thickness or test method. This behavior was consistent with other properties in terms of changes in aging mechanism or onset T_d. Again, the transition temperature of the EA9394C-2 was about 30 °C higher than that of the regular EA9394 epoxy. The transition behavior was also characterized by FT-IR, which showed the most noticeable molecular changes after aging at 260 °C in both candidates.

Based on the overall test results of the 15-day thermal aging experiment, both epoxy candidates can be considered stable up to 220 - 230 °C for a short-term exposure, and involved no noticeable changes in aging mechanisms. Thus, the maximum temperature determined for the longer-term accelerated thermal aging tests was 225 °C. Consequently, the three temperatures, 175 °C, 200 °C, and 225 °C were selected for the accelerated aging tests for more comprehensive and systematic evaluation of the candidates. The high temperature formulation, EA9394C-2, was proven for its improved thermal stability than the original EA9394 epoxy, by about 30 °C.

The 15-day thermal aging experiment of TL candidates was performed by exposing the materials to only five temperatures, 130, 160, 190, 220, and 260 °C. All aging experiments were carried out simultaneously. Various torque sample assemblies representing the three different joint types were employed for this aging experiment. According to Figure 8, all three candidates showed similar weight loss behavior against the aging temperature. The trends for all samples started with slower mass loss rates at the lower aging temperatures up to ~ 220 °C, but then followed much steeper rates as the temperature increased. This suggested that above the transition temperature, ~ 220 °C, the TL materials underwent potential changes in aging mechanism or T_d.

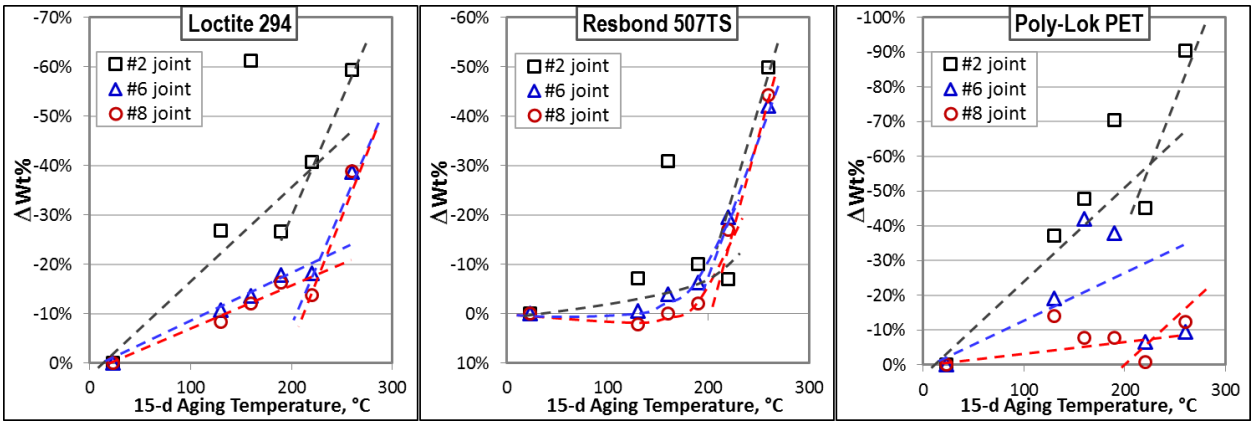

Figure 8. Weight loss trends of the three thread locker candidates as a function of aging temperature.

Mechanical performance of the TL candidates was evaluated more extensively via torque testing including failure mode analysis. Based on unaged properties of the control at various test temperatures, all three candidates showed steady torque performance up to 200 °C. The Resbond 507TS scored highest breakloose torque strength regardless of joint type. Typical effects of aging temperature on torque strengths of the candidates are illustrated in Figure 9 in #2 joint tested at both 100 and 200 °C. In most cases, regardless of TL type, the torque strengths remained stable or either slightly changed with temperatures up to ~ 220 °C. At 260 °C the rate changed was more abrupt, which may have been indicative of changes in aging mechanism. Most samples aged at 260 °C were completely blackened or charred TL residues on fasteners, which suggested thermal degradation. Resbond 507TS performed best on the blind-hole joint in the aging temperature range. The candidates also exhibited similar transition behavior in joints #6 or #8. Resbond 507TS still performed best, but Loctite 294 showed equivalent performance, particularly in prevailing torque. It should be noted that Resbond 507TS underwent the color change at somewhat lower temperatures, at around 220 °C. In addition, the systematic FT-IR analysis indicated no sign of significant thermal degradation up to 260 °C despite of the color changes in all three candidates with the exception Resbond 507TS aged at 260 °C, which showed broadening of a few major peaks. Those changes could be sign of thermal degradation as also suggested by color changes, thus Resbond 507TS can be considered thermally stable only up to 220 °C. Based on the overall test results of the 15-day thermal aging experiment, both 190 and 220 °C were selected for the 6-month long-term accelerated aging tests.

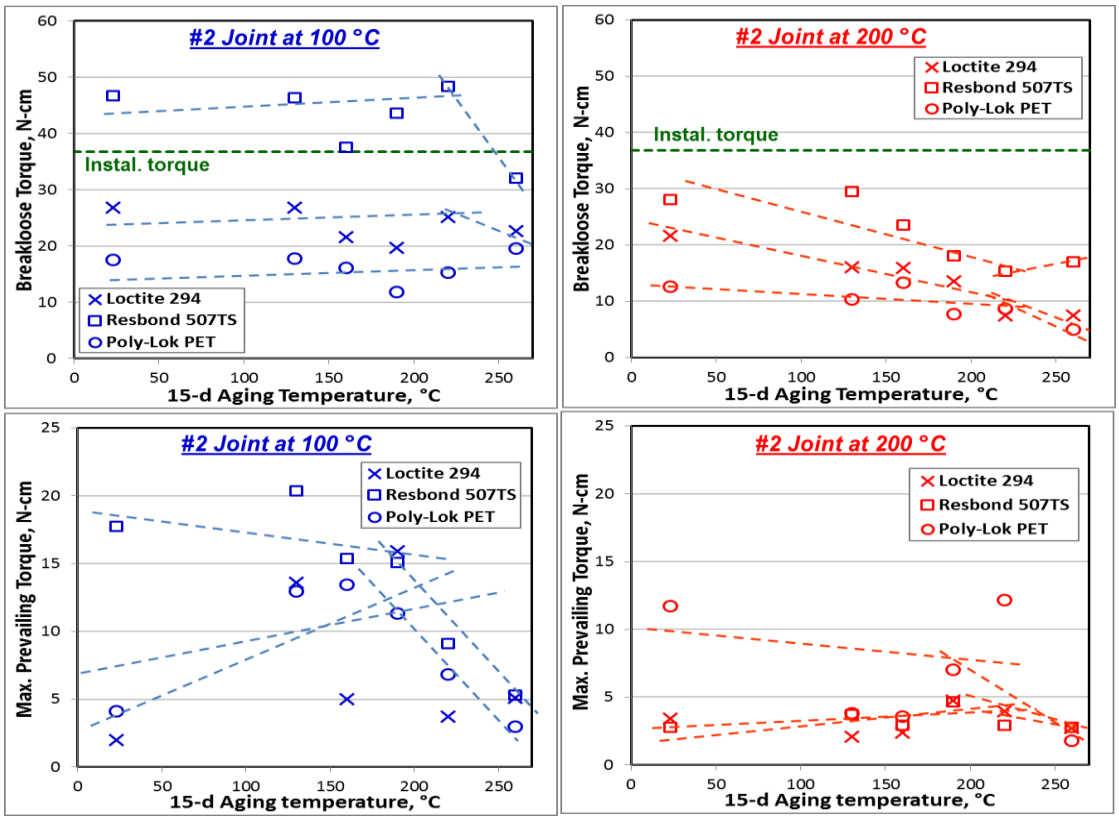

Figure 9. Typical torque strengths of thread locker candidates in #2 joint tested at 100 °C and 200 °C as a function of aging temperature.

The 15-day thermal aging testes for shrink tubing and o-ring candidates were not performed due to logistics issues. Based on the initial screening test results, the manufacturere's technical data, and maximum use temperature ratings, the same temperatures selected for the adhesive/potting candidates were selected for the 6-month long-term accelerated aging tests.

Therefore, for the candidates of adhesive/potting, shrink tubing, and o-ring, three temperatures, 175 °C, 200 °C, and 225 °C were selected while two temperatures, 190 °C and 220 °C were designated for the TL candidates. Since the selected aging tempertures were same and the aging test was conducted under the inert gas environment, the former three material types were tested together in the same experiment. For the accelerated thermal aging experiment, the extensive and systematic residual property characterizations were made at five different aging intervals including the baseline control at 0, 15, 50, 100, and 180 days.

From the 6-month accelerated aging experiment of the adhesive/potting candidates, the sheet samples aged at 260 °C (especially those aged for 100 days or longer) showed the most visible changes in both color and physical appearance where the samples completely darkened, blistered, and cracked, which were all signs of thermal degradation. Figure 10**Error! Reference source not found.** shows weight loss behavior of both candidates in either laminated thin film or thick sheet formats as a function of aging time at various aging temperatures. Overall, the EA9394C-2 samples lost more mass than AF131-2 at majority of the aging temperatures. Weight losses of the AF131-2 epoxy were well-contained up to 200 °C aging, but increased rapidly at 225 °C with increasing time due to potential thermal degradation. EA9394C-2 showed significant mass loss at aging temperatures above 200 °C, but in the case of the laminated thin film, it leveled off after 50 days. The weight loss rate of AF131-2 exceeded EA9394C-2 after about 150 days at 220 °C regardless of sample type. In general, the laminated samples mimicking the magnet bondline showed less weight losses since the only edges of the epoxy film were exposed, and thus limited diffusion paths. Overall weight loss of the EA9394C-2 was still less than that of the regular EA9394 epoxy within the aging temperature ranges studied.

From the static bonding properties of the candidates via the sub-scale sandwich lap shear specimens, Figure 11, EA9394C-2 was more stable at all aging times and temperatures up to 225 °C regardless of test temperature. The AF131-2 appeared to suffer significant property degradation when aged above 200 °C due to thermal degradation.

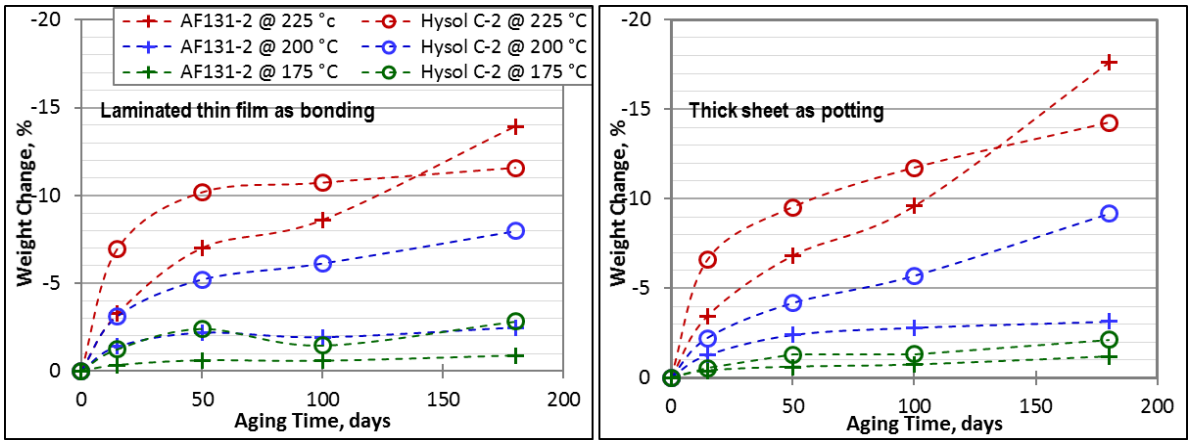

Figure 10. Weight losses of adhesive candidates as a function of the accelerated thermal aging conditions.

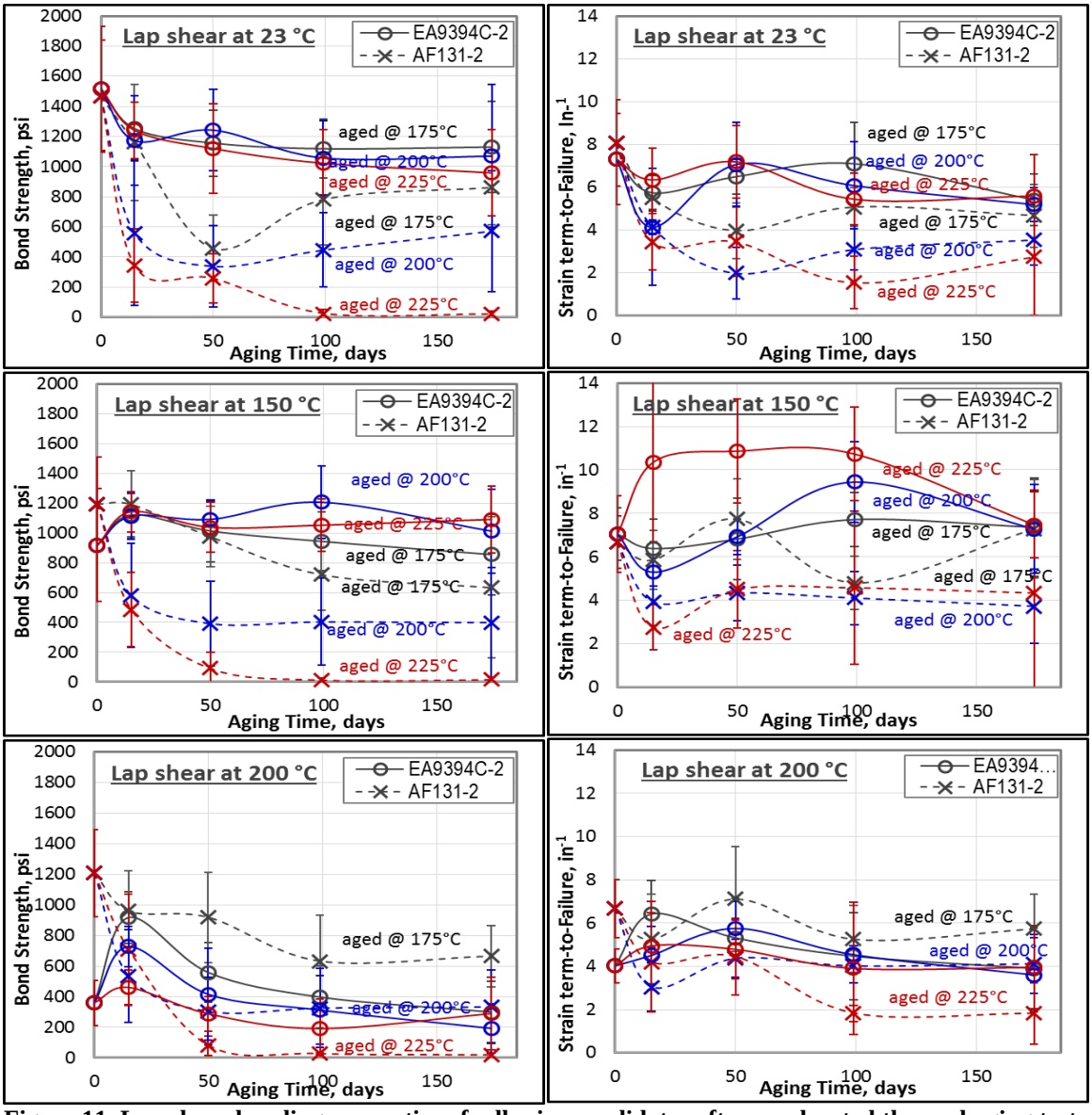

Figure 11. Lap shear bonding properties of adhesive candidates after accelerated thermal aging tests plotted against aging time.

However, the property decrease leveled off with increasing aging time for both candidates which suggested no more or less thermal degradation. Initial increases in bonding properties of the EA9394C-2, particularly at the elevated temperatures, were probably due to cure advancement. As also shown in the plots, both candidates suffered significant strength drop at 200 °C, especially EA9394C-2 regardless of aging temperature. However, the drop was associated with its intrinsic temperature capabilities of the material based on its relatively lower T_g, and adhesion mechanisms, and did not necessarily involve thermal degradation. Nevertheless, both candidates showed considerably higher bond strengths than the required strength for the magnet bonding regardless of the aging conditions or test temperature. It should be also noted that considerable differences in lap shear bonding properties were observed between the old sample batches made for the 15-day thermal aging experiment and the new batches for the 6-month accelerated aging experiment. The differences were attributed to changes in specimen fabrication conditions and procedures, testing fixtures, and overlap area measurement techniques. However, their cure states should be the same since both batches were exposed to the same cure cycles and procedures. Furthermore, the properties from the 6-month batches were more consistent in most cases. Thus, the extended property-performance evaluations for assessing long-term thermal stability in newer batches should be valid and effective since its potential effects were carefully gauged in every data analyses and interpretations.

Fatigue performance was characterized via various parameters determined from the master SN curve which included FS or endurance limit, the ratios of fatigue to static strength, the residual strength to static strength, the residual strength to fatigue strength, and the residual strain-term to static strain-term. The shape and trend of the SN curves were also characterized with the initial slope indicating load sensitivity and $\Delta\sigma$, a possible indication of any molecular structural changes due to the combined exposure of temperature and fatigue loading. In theory, $\Delta\sigma$ can be small or near zero if no changes, positive for destructive changes, such as micro-cracking, localized debond, or negative for constructive changes in terms of adhesion. In overall fatigue performance, EA9394C-2 outperformed AF131-2 epoxy regardless of the aging conditions. As shown in Figure 12, fatigue strength of EA9394C-2 was more stable and consistent against the aging conditions, and was thereby considered more thermally stable than AF131-2, as was also in the case of the static bonding properties. The AF131-2 also showed reasonable fatigue performance and thermal stability, but only up to 200 °C aging, thus it is recommended that its maximum operation temperature be limited to 200 °C. The initial slope of the SN curve generally decreased initially and leveled off with increasing aging time for most aging temperatures, which indicated that their fatigue behavior became less sensitive to the applied load and may have also related to their cure state. The $\Delta\sigma$ increased initially, but then it returned to a neutral or negative position. This was especially the case for the EA9394C-2 epoxy, where the trend increased with aging time, which was indicative of no major structural changes by fatigue loading in both candidates. Other various fatigue performance parameters suggested that both candidates performed better under fatigue loading than static loading, especially with increasing aging time in most aging temperatures.

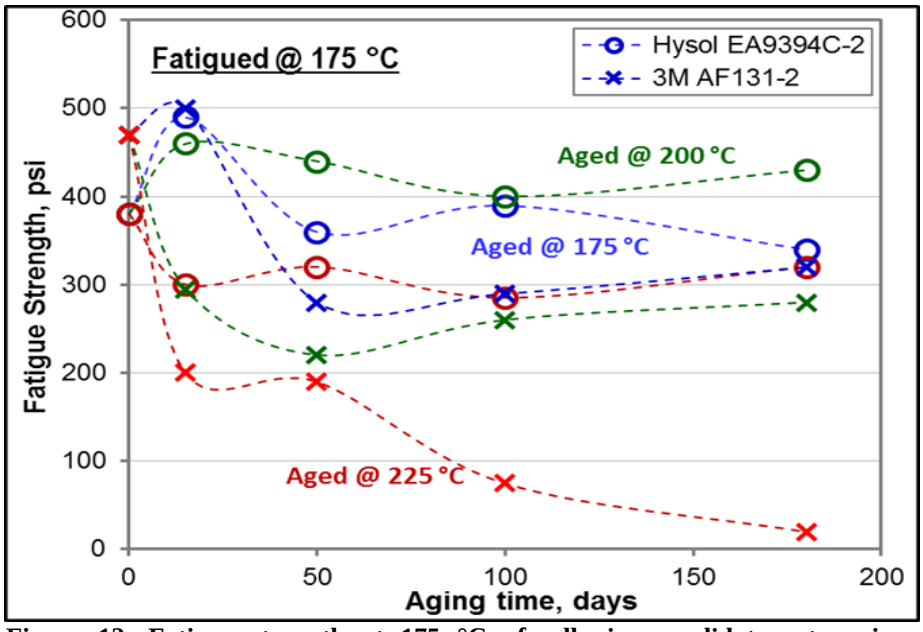

Figure 12. Fatigue strength at 175 °C of adhesive candidates at various accelerated thermal aging conditions

No sign of fatigue-induced bonding integrity degradation was observed in both candidates regardless of the aging conditions. In most cases, the residual-to-static strength ratio was even higher than 1.0, which suggested bonding integrity was improved with fatigue testing.

For both candidates, the T_g increased initially at the early aging stage mostly due to cure advancement. The behavior then either leveled off or continued to increase with increasing aging time, and then decreased significantly when aged at 225 °C due to thermal degradation, particularly for the AF131-2. Other thermal properties including T_d, G', and ΔWt% at 700 °C as well as the FT-IR analysis showed similar behavior when more dramatic changes occurred after aging at 225 °C regardless of sample configuration or format. The changes were greater for the AF131-2 in most cases, where changes in the FTIR spectra were more than likely the result of thermal degradation at 225 °C, but EA9394C-2 also showed some visible changes from 200 °C aging, especially from the thick sheet sample. However, the laminated thin film sample representing magnet bonding did not show any changes when aged at 200 °C.

In most residual property characterizations, changes in properties seemed to level-off or stabilize after 180 day aging at all aging temperatures studied, and thus the 180-day properties can be considered as representative values per each aging temperature for longer-term predictions. All of the residual properties at the end of 180 day aging experiment were plotted together as a function of aging temperature for more direct and practical comparison in terms of percent change from the respective baseline control property, Figure 13. As can be seen in the plot, AF131-2 suffered greater reductions in most properties than EA9394C-2, with sharper, more distinctive transitions in the reduction rates at 175 – 200 °C, the temperature that may be used as the upper limit for long-term applications. On the other hand, EA9394C-2 adhesive showed better thermal stability without significant property reductions up to 225 °C, but low bond strengths at 200 °C have to be counted for when determining its upper limit. It should be also noted that the larger changes either, up or down, indicate the greater effects of the thermal aging, but whether the changes is positive or negative have to be determined by the nature of the properties.

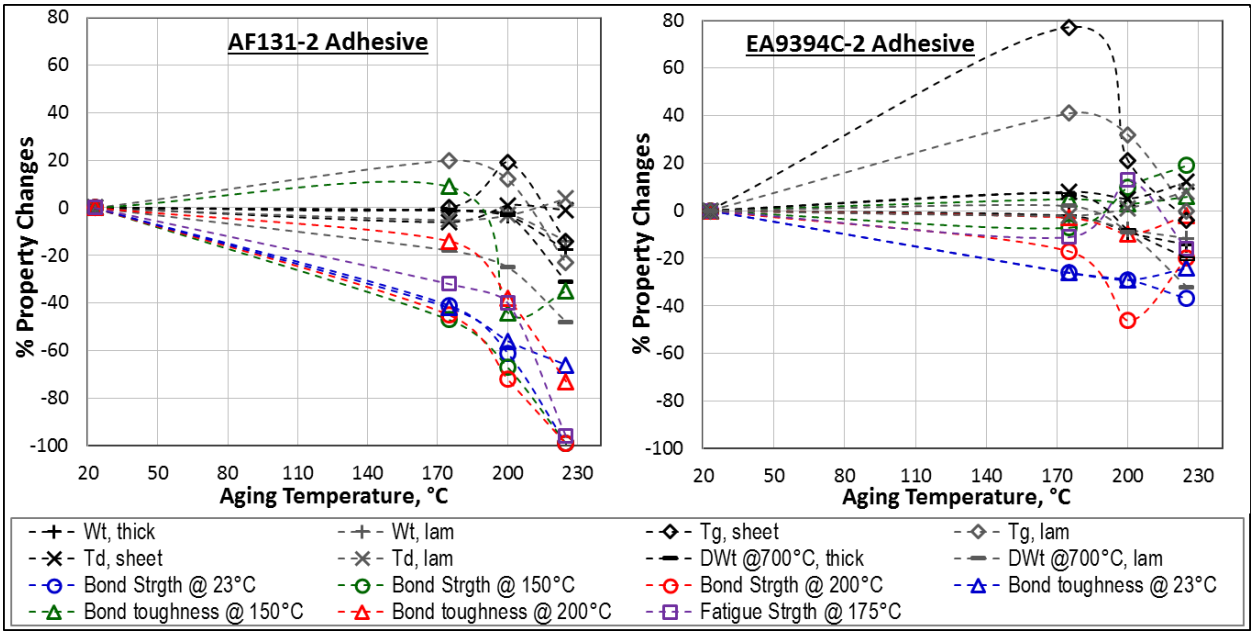

Figure 13. Overall percent changes in various properties of adhesive candidates after 180-day aging as a function of the accelerated thermal aging temperature.

From the 6-month accelerated aging experiment of the TL candidates, their total weight losses were rather significant, ~ 15 wt% up to 40 wt% or higher, compared to other Stirling organic materials studied. The mass losses depended not only on aging temperature and time, but also on joint type, Figure 14**Error! Reference source not found.**. For both Loctite 294 and PET, the #2 joint with blind-hole configuration resulted in the highest weight loss regardless of aging temperature. The mass loss of Resbond 507TS was more dependent upon aging temperature regardless of joint type. In most cases, the rate of mass loss either decreased or leveled off with increasing aging time for both aging temperatures. Whether the weight losses were due to thermal degradation, chemical reactivity,

or just benign outgassing will be further assessed along with other residual property evaluations and TCIOP in-situ outgassing analyses.

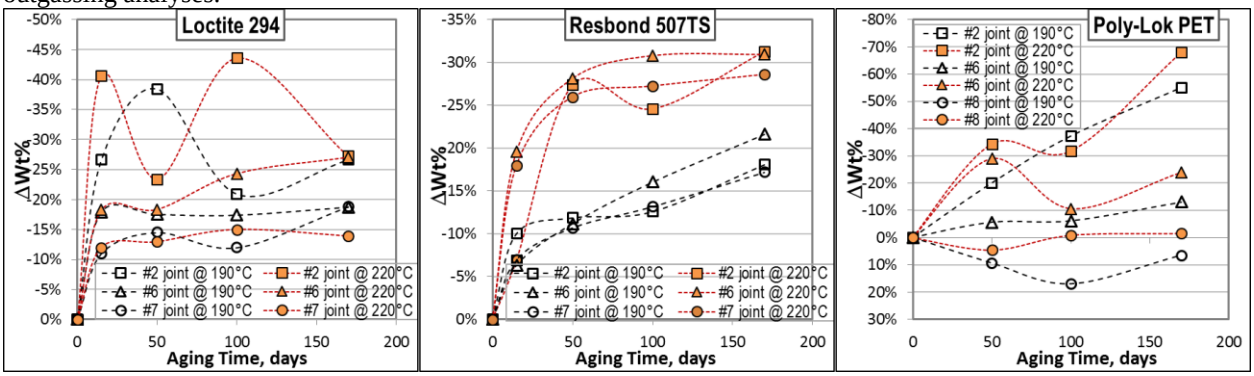

Figure 14. Overall weight losses of thread locker candidates against the accelerated aging conditions.

The typical effects of accelerated thermal aging on torque strengths of the TL candidates in the #6 joint are summarized in Figure 15. The effects varied somewhat with different joint types, but their overall performance followed similar trends. For the torque strengths, Resbond 507TS performed best regardless of aging conditions or joint type, especially at 100 °C. Resbond was the only candidate generating 100 °C breakloose torques greater than the installation torques in all three joint types. Loctite was the next best candidate, but with considerably lower breakloose torques. In some cases, the torque strength of most candidates increased with aging time, especially up to 50 days aging, with the exception of joint #2. Overall, the torque strengths of all three candidates were not significantly impacted at both aging temperatures up to 220 °C. At 200 °C, the Resbond 507 TS suffered the most loss of breakloose torque among all candidates even though its strength was still higher than other candidates. Overall, their torque strengths at 200 °C were considerably lower than the installation torque.

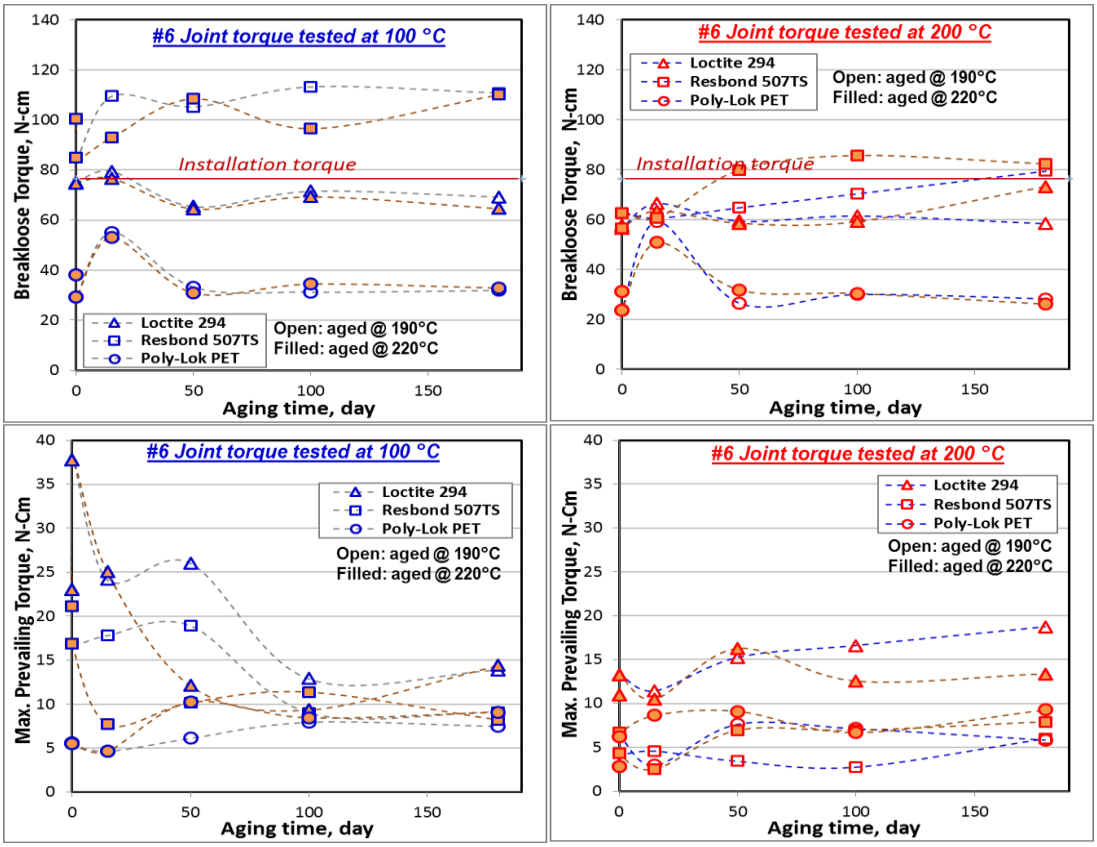

Figure 15. Torque strengths at 100 °C and 200 °C of thread locker candidates in #6 joint as a function of the accelerated thermal aging conditions.

For all candidates, their prevailing torques were much lower than their breakloose torques or installation torque except Loctite in the #7 joint, which was less affected by the higher test temperature of 200 °C than breakloose torques. The breakloose torque at 100 °C in the joint type #7 or #8 with the thru-hole configuration was highest among all joint types, especially in terms of the percent installation torque. In joint #7 or #8, prevailing torques of the candidates were also significantly higher, particularly Loctite and Resbond. In many cases of the Resbond 507 TS in #7 joint, their prevailing or maximum torque strength was greater than torque strength of the fastener itself, which lead to failure at the fastener head during torque testing. Regardless of TL type, the joint #2 with blind-hole configuration always showed less favorable failure modes, either in the adhesive or mixed modes. Loctite 294 and Resbond 507 TS in #7 joint showed more favorable cohesive failure modes, but the latter seemed to be more prone to thermal degradation. Analysis of the FT-IR spectroscopy data after torque testing indicated that Resbond underwent potential molecular changes in agreement with thermal degradation, especially when aged at 220 °C or at longer aging times, regardless of joint type. These observations were somewhat consistent with the results of OM failure mode analysis. Both Loctite and PET were thermally stable up to 220 °C aging for the entire aging time.

From the 6-month accelerated aging experiment of the shrink tubing candidates, SRFR was slightly discolored, especially when aged at 225 °C, but no visible physical changes were observed. The ETFE material seemed to become less elastic, and sometimes adhered together or with the Z1028 o-ring with increasing aging time or temperature. Based on the extensive mechanical performance evaluation via notched tensile properties in Figure 16, ETFE performed better and more thermally stable than SRFR regardless of sample direction (either axial or radial) and test temperature (25 °C or 200 °C). Generally, the thermal aging caused considerable deterioration of the properties, but the changes mostly occurred at the early stage of aging and seemed to level off with increasing aging time for all three aging temperatures. SRFR suffered greater deterioration in both ultimate strength and elongation than ETFE in most cases. The rate of deterioration in strength in SRFR continued to increase instead of leveling-off when aged at 225 °C, while strength of ETFE either increased or remained unchanged. In general, the notch strength of ETFE was about three to four times higher in both directions than SRFR regardless of aging conditions or test temperature. In contrast, the ultimate elongation properties of both materials were similar in most cases.

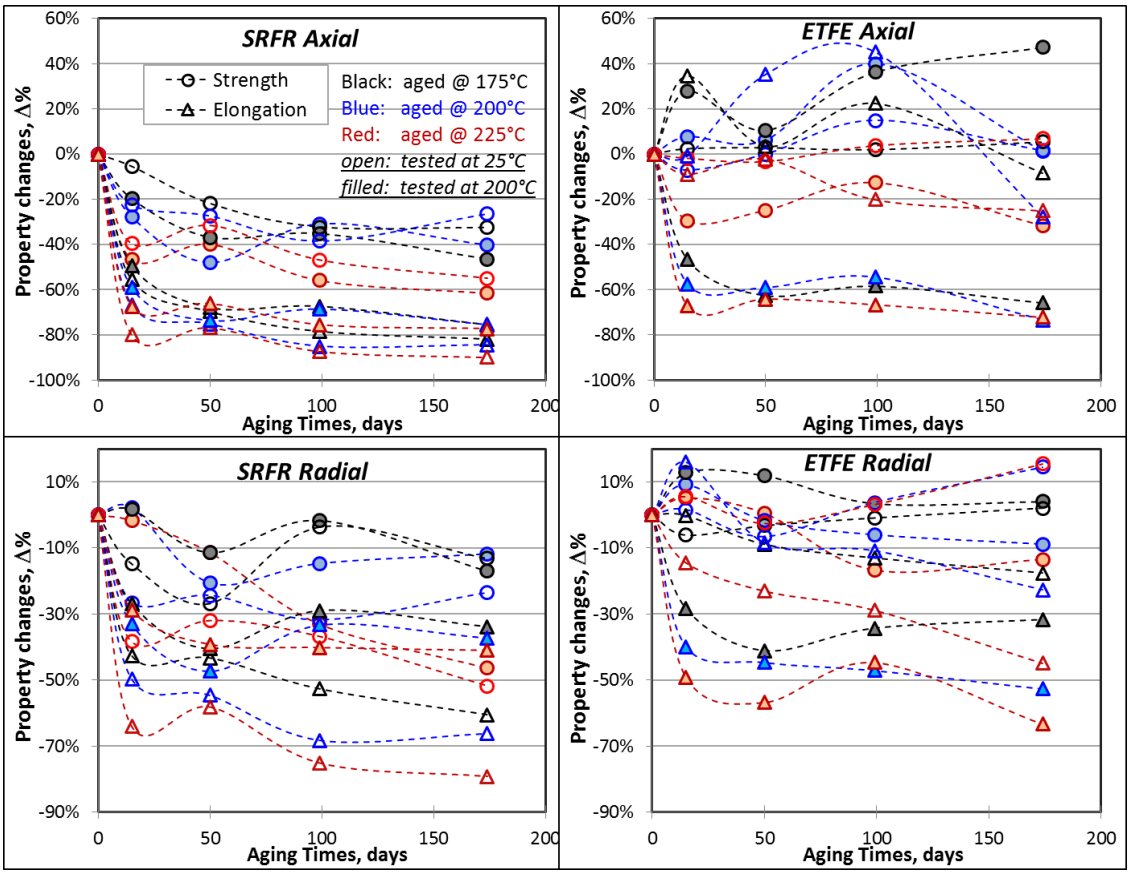

Figure 16. Changes in notched tensile properties of shrink tubing candidates in either axial or radial direction as a function of the accelerated thermal aging conditions.

Similar to the adhesive evaluation, all of the residual properties at the end of 180 day aging in percent change from the respective baseline control properties were plotted together as a function of aging temperature, Figure 17. Overall, SRFR suffered more undesirable reductions in more properties with increasing aging temperature than ETFE. On the other hand, ETFE shrink tubing showed better thermal stability or positive changes in more properties, even though the low ultimate elongation at 200 °C have to be considered when determining its upper limit. Examining details of specific properties, the weight loss of ETFE with aging was less than 0.5 wt% up to 200 °C at 180 days, but increased gradually with increasing aging time at 225 °C up to 1.8 wt% after 180 days. In the case of SRFR, the mass loss gradually increased starting at approximately 200 °C and increased to 1.44 wt% at 180 days, reaching ~ 2.8 wt% at 225 °C by 180 days. Its rate further increased with increasing aging time. For both candidates, T_g or T_m were not significantly affected by aging regardless of temperature and time, but T_t and E' ratios by DMA varied considerably with aging in both sample directions, especially for SRFR. In the case of T_d, SRFR showed substantial changes, mostly at the beginning of aging for all three aging temperatures, and then leveled off with increasing aging time. The ETFE material showed no significant changes regardless of aging time and temperature. From both TGA and iso-TGA characterizations, the outgassing potentials of SRFR were greater than Z1028 and was more affected by thermal aging. The char yield at 700 °C of ETFE, ~ 6 wt%, was little affected by the thermal aging regardless of temperature or time, but SRFR showed considerable decrease, especially at 225 °C, from ~83 % to ~ 75%. The systematic and quantitative FT-IR analysis, including both inner and outer surfaces, indicated that SRFR suffered possible chain scissions upon thermal degradation when aged at 225 °C, especially with increasing aging time. The molecular network structure of ETFE was considered to be thermally stable up to 225 °C aging.

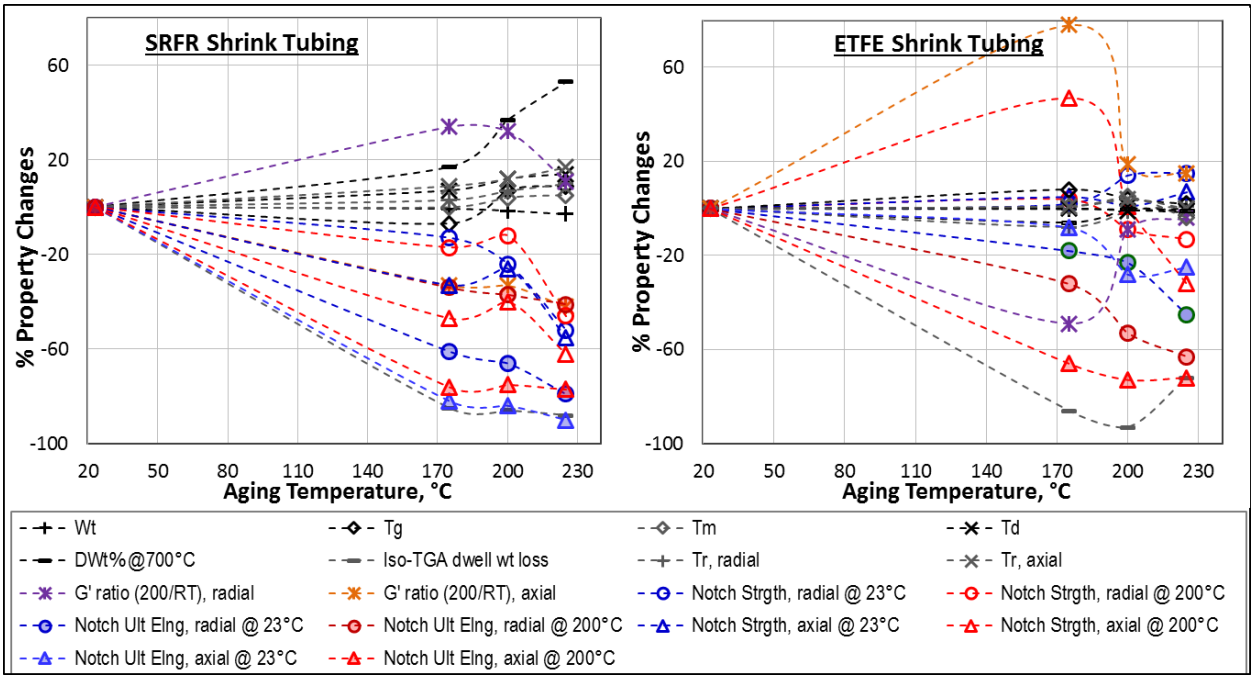

Figure 17. Overall percent changes in various properties of shrink tubing candidates after 180-day aging as a function of the accelerated thermal aging temperature.

From the 6-month accelerated aging experiment of the o-ring candidates, S1151 o-ring was slightly discolored, especially after 100 days at 225 °C, but no visible physical changes while Z1028 seemed to become less elastic, and sometimes sticking together, especially with increasing aging time or temperature similar to ETFE shrink tubing, as a same family of fluoropolymers. Based on the extensive mechanical performance evaluation via hardness, compression-set (C_B), and tensile properties, Z1028 o-ring outperformed S1151 in most cases, especially in terms of thermal stability. Z1028 was thermally stable up to 225 °C aging, while the thermal stability of S1151 considerably deteriorated at the aging temperature above 200 °C. Hardness of the S1151 o-ring increased with the thermal exposures, more significantly with higher aging temperatures (i.e., ~ 4% at 175 °C vs. ~ 7 % at 200 °C or ~9 % at 225 °C at the end of 180-day aging). On the other hand, the Z1028 o-ring showed no changes in hardness regardless of aging temperature and time, less than ±1 %. For both candiates, thermal aging exposure lowered the

compression-set significantly, where the material more than likely became more elastic due to the additional chemical cross-linking during aging, and ultimately improved the compression-set. At the same time, thermal aging might decrease physical cross-link density, due to the formation of crystallites or densely packed blocks. In general, an appropriate range of cross-link density is needed for the optimum compression-set performance. Overall, the Z1028 o-ring showed better compression-set performance than S1151 regardless of aging temperature and time. In most cases, room temperature tensile properties of the Z1028 o-ring were superior to those of S1151. At elevated temperatures 150 and 200 °C, the S1151 o-ring exhibited slightly better than or equal properties to the Z1028 o-ring. Similar to hardness, changes in Young's modulus were much less in Z1028 o-ring regardless of aging conditions or test temperature. Significant increase in Young's modulus of S1151 consisted with changes in other properties, such as compression-set and hardness, are indicative of poor thermal stability. Tangent modulus of both o-ring materials showed the same trends as their Young's modulus. Regardless of test temperatures, the S1151 o-ring suffered a major drop in ultimate strength or elongation-to-failure when aged at 225 °C, Figure 18. Strength of the Z1028 o-ring at test temperatures up to 150 °C was mostly unchanged regardless of aging temperature and time. Changes in tensile strength at 200 °C altered with aging time in both o-ring materials, where an initial decrease was observed followed by an increase in strength with increasing aging time for all three aging temperatures. In both o-ring materials, the ultimate elongation regardless of test temperature was reduced initially with aging, but then stabilized with increasing aging time for all three aging temperatures. In most cases, S1151 o-ring suffered greater loss of ultimate elongation, especially when aged at higher temperatures above 200 °C. The changes in ultimate elongation of Z1028 o-ring were neglible at the test and aging temperatures, which suggested good thermal stability.

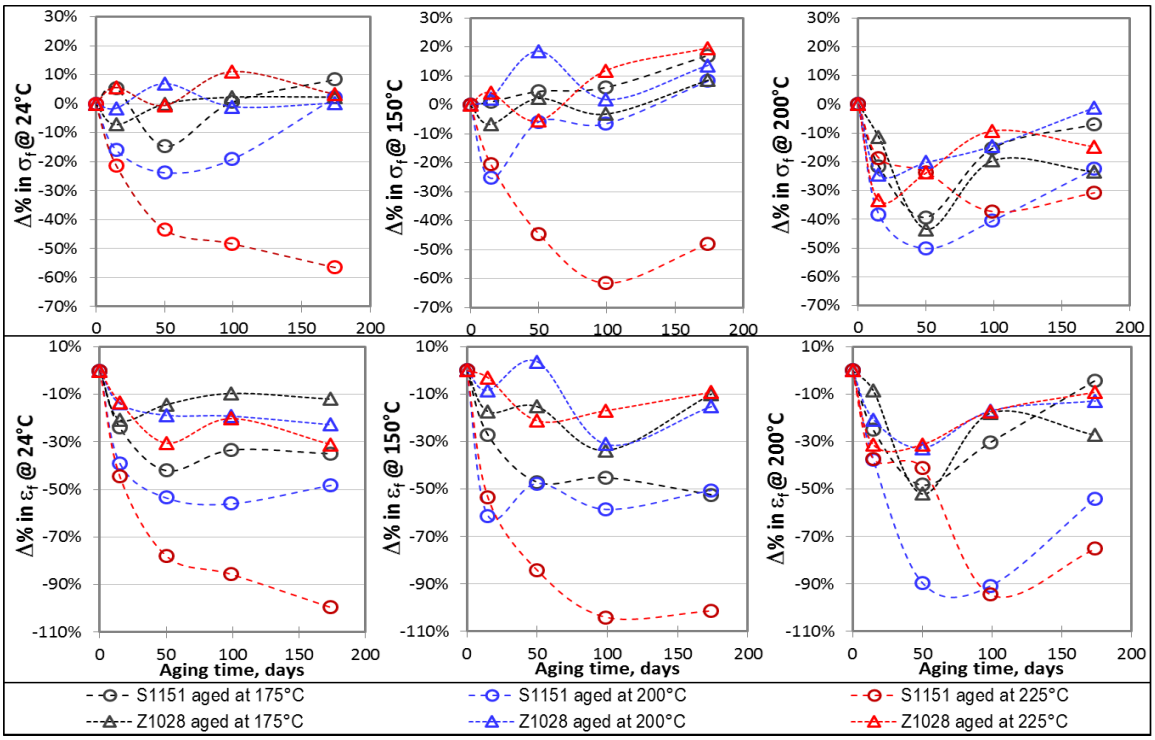

Figure 18. Changes in tensile properties (ultimate strength and elongation-to-failure) of o-ring candidates as a function of the accelerated thermal aging conditions.

Finally, all the 180-day properties of the candidates were plotted together in terms of percent changes from their respective controls as a function of aging temperature in Figure 19. It is evident that properties of the Z1028 o-ring were considerably more thermally stable than S1151 in most cases. Accessing details of the specific properties, the weight loss of Z1028 with aging was negligible regardless of aging time and temperature, while the S1151 material lost about 2 wt% at 200 °C and more than 5 wt% at 225 °C, respectively, at the end of 180-day aging experiment. At 175 °C, the weight loss of S1151 was leveled off at ~ 0.7 wt%. For most of the thermal properties including T_g, T_m, T_{exo}, T_d, and ΔH, S1151 showed considerable changes with aging, especially at 225 °C while Z1028 showed no significant changes regardless of aging time and temperature. From both TGA and iso-TGA characterizations, the outgassing potentials of S1151 were greater than Z1028 which showed negligible changes up to 225 °C. For both

candidates, their char yield at 700 °C did not show significant compositional changes following exposure to thermal aging. The systematic and quantitative FT-IR molecular network structure analysis indicated that S1151 suffered from possible chain scissions upon thermal degradation when aged at temperatures above 200 °C, especially with increasing aging time while Z1028 showed thermally stable molecular networks up to 225 °C aging.

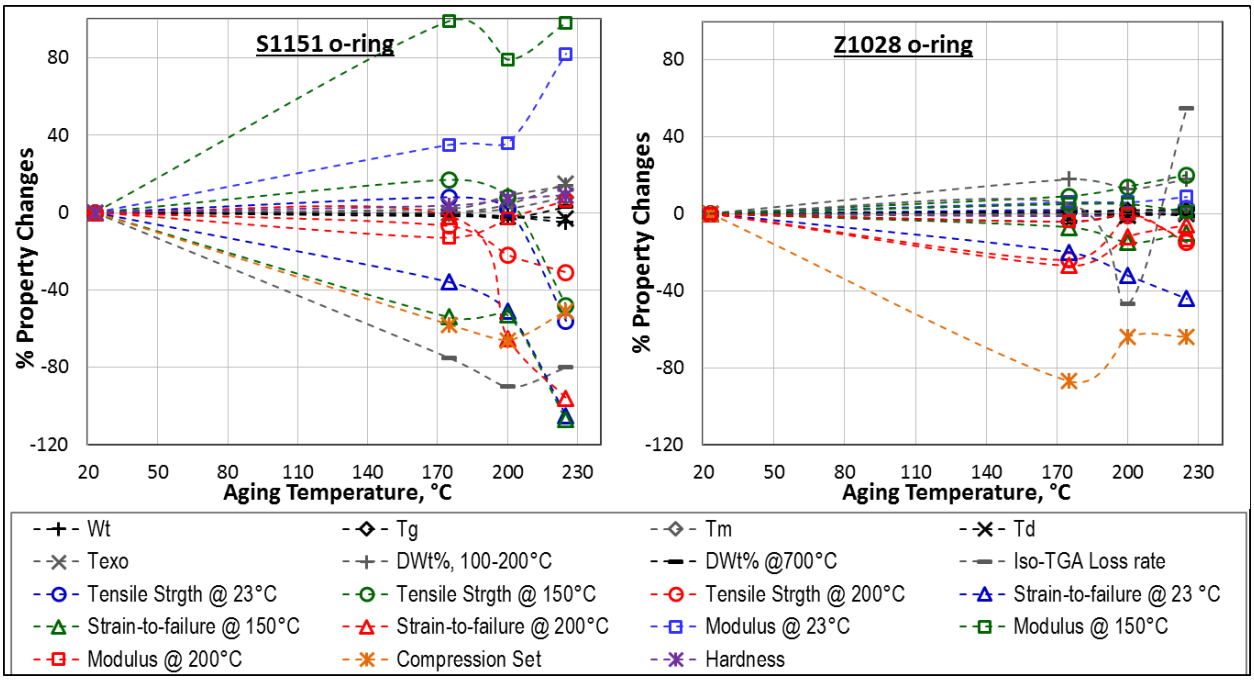

Figure 19. Overall percent changes in various properties of o-ring candidates after 180-day aging as a function of accelerated thermal aging temperature.

3. TCIOP Material Compatibility

Specific objectives of this task were to determine outgassing behavior of the down-selected candidates under the typical Stirling convertor pre-mix gas environment and the effects of outgas on their properties and performance to assess material compatibility for the Stirling application. This TCIOP material compatibility assessment was made with two step approaches, i.e., in-situ outgas analyses and residual property characterizations, consistently and systematically for all material types. The in-situ outgas analyses combined three different gas analysis techniques, RGA, GC/TCD, and FT-IR, thus the results were compared and validated.

For adhesive/potting candidates, the typical gas compositions at the beginning of TCIOP testing via RGA consisted of the pre-mixed Stirling convertor gases (i.e., H_2, O_2, N_2, CO_2, He), and possible residual air contaminants (CH_4, H_2O, Ar, CO, Ne) and some higher Mw species suspected of pump oil. Concentrations in most gas species were comparable between the adhesives during the TCIOP exposures, but all three gas analyses confirmed that the EA9394C-2 increased concentrations of CH_4, H_2O, CO, and CO_2 with increasing exposure temperature and time while the AF131-2 caused no significant changes, Figure 20. Most increases occurred at 200 °C exposure and seemed to be accompanied by decreases in H_2 and O_2, and possibly linked to its cure advancement. This result agreed with the higher weight loss of the EA9394C-2 at 200 °C from the 6-month aging experiment. Based on FT-IR gas analysis, EA9394C-2 also produced additional outgases at temperatures above 150 °C indicated by a few new peaks at ~1033, 966, 931, or 816 cm^{-1} at temperatures above 150 °C. They were suspected to be from the fillers or unsaturated alcohols, CH-O-H, which might result from either molecular rearrangements, possible outgas-epoxy interactions, or onset of thermal degradation. However, their actual concentration and impact on material compatibility or durability could not be assessed with the data available to date.

The systematic residual property characterizations of the TCIOP tested samples, especially when the results were directly compared to those of the same samples undergone the similar thermal exposures but under inter gas environment, suggested that the EA9394C-2 epoxy seemed to be more affected by the Stirling gas environment than the AF131-2 epoxy in terms of slightly higher weight loss, lower bonding properties, and more FT-IR molecular network structural changes, so might be less compatible. However, the differences were rather small or insignificant in most cases. On the other hand, most thermal properties indicated that the pre-mix gas accelerated cure

advancement of the epoxies through additional cross-linking reaction and/or possible oxidation in terms of considering the slightly higher T_g, % cure, and rigidity at 200 °C. More specifically, the T_d of the EA9394C-2 was not negatively affected by the TCIOP exposure.

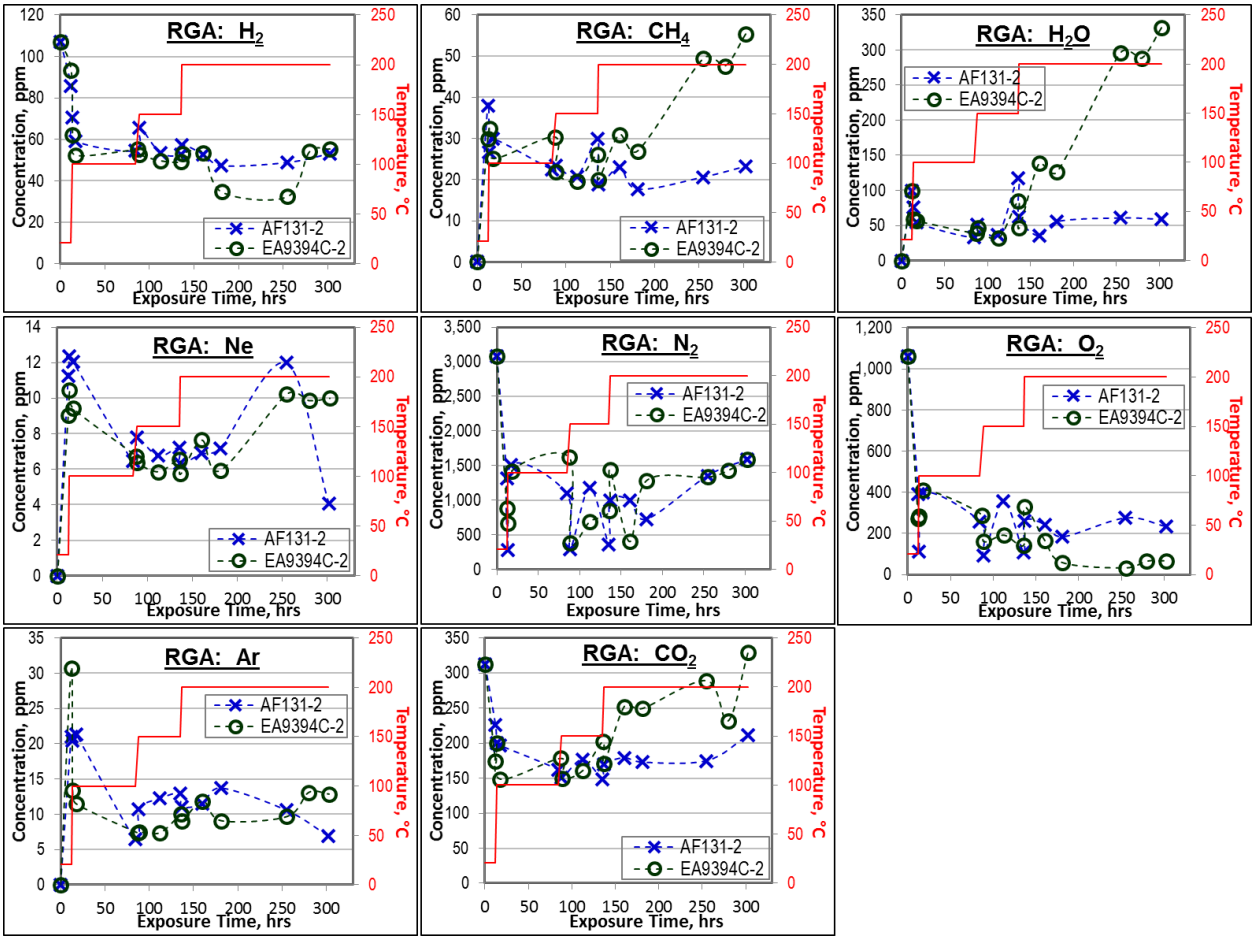

Figure 20. Overall changes in concentrations of various outgas species by RGA during TCIOP exposures of adhesive candidates.

For TL candidates, while starting with the similar gas compositions as the previous adhesive testing, the outgassing behavior of the TL materials was directly compared to that of the pre-mix gas alone as a baseline which showed no inter-gas reactions regardless of the TCIOP exposure conditions. Based on consistent results of RGA, GC/TCD, and FT-IR analyses, both candidates increased CO_2 concentration gradually at the expense of O_2, mostly during 200 °C exposure, Figure 21, which seemed to suggest outgassing of C from the TL materials. Increase in H_2O was also observed at the 200 °C exposure in both candidates, especially for Loctite 294. It was apparent that those increases resulted from additional outgassing from the TL materials, but it was not clear whether or not the outgassing was due to either thermal degradation, degassing of volatiles, or by-products of additional cure. In addition, FT-IR analysis uniquely revealed the formation of CO and $-CH_3/-CH_2-$ compounds at 200 °C exposure and their concentrations increased with increasing exposure time in both candidates, Figure 22. However, their formation seemed to be transitional due to their high reactivity, especially since they were not registered by RGA or GC/TCD.

From the systematic residual property characterizations of the TCIOP tested samples, there was no additional outgas-induced weight losses in both candidates in joint #2 with the blind-hole configuration, but in joint #8 with thru-hole configuration, slightly higher weight losses of Resbond 507TS after TCIOP exposures than the trends observed under the inert gas thermal exposures, suggested possible thermo-chemical degradation. However, their torque strengths, failure mode, and FT-IR molecular network structure were not negatively affected by TCIOP exposure in both candidates. This suggested that whether the joint was blind-hole or thru-hole configuration, exposure to the outgases during TCIOP test didn't degrade or change the material excessively.

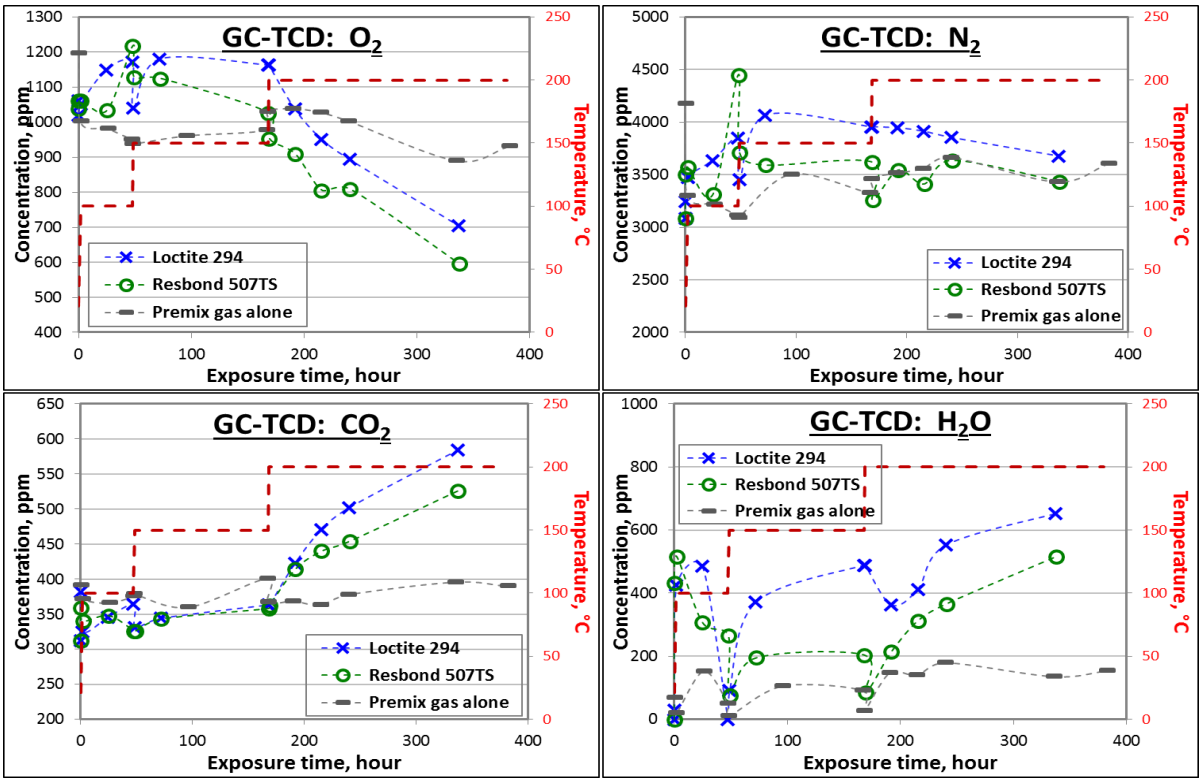

Figure 21. Overall changes in concentrations of various outgas species by GC/TCD during TCIOP testing of thread locker candidates.

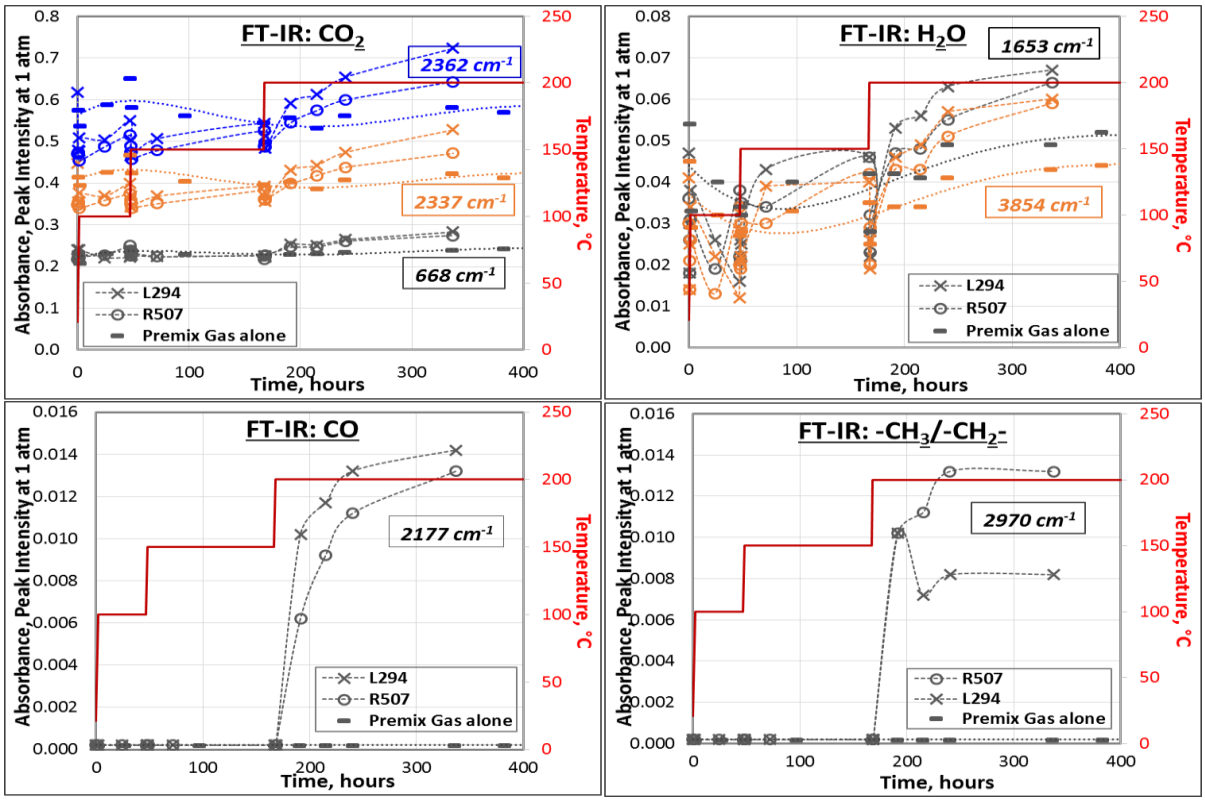

Figure 22. Absorbance peak intensity or concentration changes of outgas species by FT-IR during TCIOP testing of thread locker candidates.

For shrink tubing candidates, based on the same quantitative analyses used previously, Figure 23 illustrated that ETFE showed no significant changes in outgassing with the TCIOP exposures up to 200 °C. On the other hand, SRFR showed a steady increase of CO_2 at the loss of O_2 from the major gas species, and also an increase in CH_4 and H_2O. Most changes occurred at 200 °C exposure, and seemed to suggest outgassing of C and H_2 from the silicone material. As shown in Figure 24, FT-IR analysis revealed that SRFR formed new outgases such as -CH_3/-CH_2- and more prominently silicone vapor, especially at 200 °C. The aforementioned species concentrations rapidly increased with increasing exposure time, which was a clear indication of thermal degradation. ETFE also caused formation of new outgas species, CO, -CH_3/-CH_2-, and C-F that appeared at 200 °C and increased with exposure time even though their intensities were rather small.

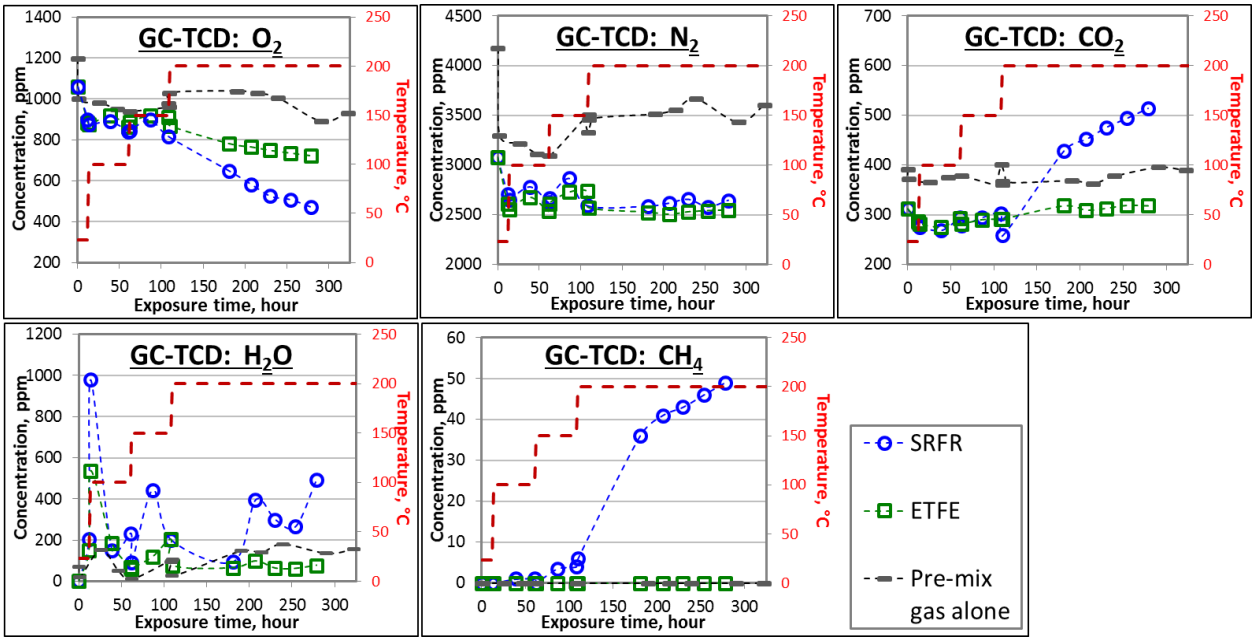

Figure 23. Overall changes in concentrations of various outgas species by GC/TCD during TCIOP testing of shrink tubing candidates.

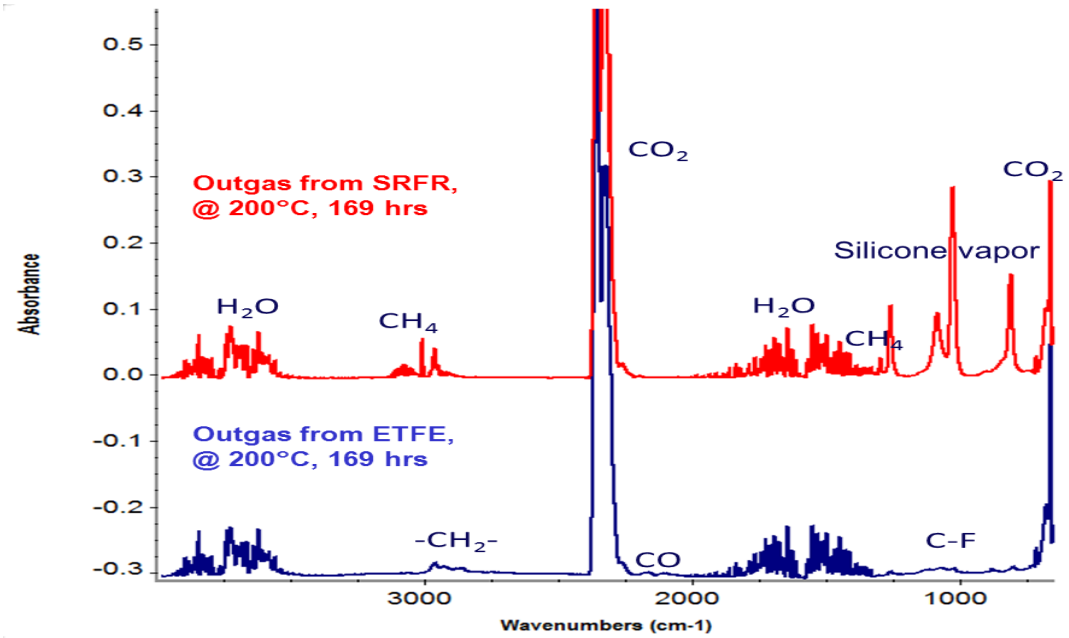

Figure 24. Typical FT-IR spectra of outgas during TCIOP testing of shrink tubing candidates and peak identifications based on NIST database.

From the systematic residual property characterizations of the TCIOP tested samples, most thermal properties and outgassing potentials after the TCIOP exposures were rather insignificant in both candidates, but consistently greater in SRFR. Furthermore, SRFR showed significant deterioration of its notched tensile properties after the TCIOP exposures compared to those of the baseline controls which was indicative of apparent material degradation due to both temperature and outgas exposures. In the case of ETFE, notched strengths were not negatively affected by the TCIOP exposure in both axial and radial direction, but the elongation at failure decreased considerably after the TCIOP exposures. Overall, ETFE performed better than SRFR, and was determined to be more compatible. FT-IR analysis of the molecular network structure of the TCIOP exposed SRFR indicated oxidation and possible side-chain rearrangement, while ETFE remained relatively unchanged.

For o-ring candidates, following the same outgassing behavior characterizations, it was found that there were no significant changes in concentrations of major gas species, such as CO_2 or O_2 during the entire TCIOP testing for both candidates unlike shrink tubing candidates even though candidates of both material types were from the similar polymer families. However, based on FT-IR analysis, S1151 like SRFR caused various new outgases such as CO, -CH_3/-CH_2-, and more prominently silicone vapor at 200 °C and their concentrations rapidly increased with increasing exposure time, which signified thermal degradation. On the other hand, Z1028 samples caused no visible changes in outgas composition and maintained good thermal stability and material compatibility during the entire TCIOP test.

From the systematic residual property characterizations of the TCIOP tested samples, changes in most thermal properties and outgassing potentials from those of baseline controls were rather insignificant in both candidates, but greater in S1151. TCIOP exposure lowered compression-set properties of both o-ring candidates, but greater changes were observed in S1151 (-38%) than Z1028 (-9%). Overall, Z1028 maintained better compression-set property, which were less affected by TCIOP exposure. In general, changes in tensile properties due to the TCIOP exposure were greater in S1151 than Z1028. TCIOP exposure made the S1151 material harder and more brittle, which was undesirable for an o-ring. Tensile properties of Z1028 were not significantly affected by the TCIOP exposure. FT-IR analysis of the TCIOP exposed S1151 indicated oxidation and possible side-chain rearrangement, while Z1028 showed little to no change.

V. Summary and Conclusions

Multi-step evaluation processes were successfully conducted to screen and down-select the most capable high temperature candidates for various organic materials for use in future high performance, high temperature Stirling convertors, particularly in adhesive/potting, TL, shrink tubing, and o-ring applications. As a part of the evaluation, processing and installation conditions of the candidates have been optimized for their applications. The application limits of all material candidates were also identified based off the extensive property and performance data.

For the adhesive/potting application, the EA9394C-2 showed better thermal stability than the AF131-2 while the latter had slightly better material compatibility. The upper application limit based on the thermal stability was 180 – 200 °C for the AF131-2 and ~ 225 °C for the EA9394C-2. However, for both adhesive candidates, the low static bond strengths at 200 °C have to be acounted for when determining more practical upper limits. Neither epoxy shall be recommended for the use temperatures higher than 225 °C. Based on the thermal stability, overall bonding performance, handleability, processability and multi-functionality, and material availability, the EA9394C-2 epoxy was recommended as the final candidate for the future high temperature convertors. Presently, the highest service temperature of the EA9394C-2 can be 200 - 225 °C, but this temperature range shall be further validated by the synergistic durability life testing (SDLT).

For the TL application, all three TL candidates showed reasonably good thermal stability and material compatibility, but based on overall locking performance the Resbond 507TS was recommended as the final candidate for the future high temperature convertors. The upper application temperature based on the extensive evaluations should be ~ 200 °C for Resbond 507TS, or ~ 225 °C for both Loctite 294 and PET. The highest service temperatures recommended for those candidates in this report shall be further validated by the synergistic durability life testing (SDLT) in future.

For the shrink tubing application, ETFE shrink tubing showed better thermal stability and material compatibility than SRFR shrink tubing, thus ETFE was recommended as the final candidate for the future high temperature convertors. The upper application temperature based on the extensive evaluations should be considerably lower than 200 °C for SRFR shrink tubing, or ~ 200 °C for ETFE shrink tubing.

For the o-ring application, the Z1028 o-ring showed better thermal stability and material compatibility than S1151 o-ring, thus Z1028 was recommended as the final candidate for the future high temperature convertors. The upper application temperature based on the extensive evaluations should be considerably lower than 200 °C for

S1151 o-ring, or ~ 225 °C for Z1028 o-ring. The highest service temperatures recommended for those candidates in this report shall be further validated by the synergistic durability life testing (SDLT) in future.

VI. Future Work Plan

Selection of the best candidates thus far was primarily based on the extended thermal aging experiments performed under an inert gas environment even though TCIOP tests were conducted under the Stirling convertor simulated gas environment for a short duration. As illustrated in the overall program plan in Figure 1, the final candidates will be further evaluated and validated via the synergistic durability life tests (SDLT) after combining all organic materials involved in a typical Stirling convertor in tightly sealed high pressure aging system capable of ~ 1000 psi up to 300 °C to simulate the actual Stirling service environment more closely. The tests will consist of radiation exposures, gamma and neutron, and subsequent thermal aging up to 3 years at three temperatures that have to be determined. Three aging intervals, for example 4 months, 1 year, and 3 years, are planned for outgas analyses and the extensive residual property characterizations. Once they are validated, the final process and installation optimizations, and implementation optimizations will be also followed.

Acknowledgments

This paper presented an overview of extensive work started at 2012 which involved numerous dedicated collaborators and contriubtors of whom are greatly appreciated by the author. They include Daniel Scheiman, Paula Heimann, and Andrew Ring from Ohio Aerospace Institute/NASA-GRC on-site contractor; Chris Burke from SLI/NASA-GRC on-site contractor, D. Jordan McCrone, GRC-LMA/VPL; Robert Pelaez, Sal Oriti from NASA-GRC; Tim Ubienski, Tony Kapucinski, GRC-FTH/SLI; Mike Gorbulja from KOL-CAP Manuf.; Kerry Arnold, Cliff Fralick et al. from Sunpower, Inc.; Mike Booker, CTL Inc.; Steve Hassman, Long-Lok Corporation for preparing; and Samuel Slingluff, summer interns at NASA-GRC. The author also thanks Scott Wilson, Wayne Wong, Terry O'Malley, Jim Withraw, Lee Mason for project guidance and management, and a special thanks to Tiffany S. Williams for reviewing various reports and this paper. This work has been sponsored by the GRC-RPS program office with funding from Science Mission Directorate (SMD).

References

[1]Dudzinski, L.A., Hamley, J.A., McCallum, P.W., Sutliff, T.J., Zakrajsek, J.F., "NASA's Radioisotope Power Systems Program Status," In: *11 th International Energy Conversion Engineering Conference (IECEC) proceedings*. 14-17 Jul. 2013; San Jose, California

[2]Hibbard, K.E., Mason, L.S., Ndu, O., Smith, C., Withrow, J.P., "Stirling to Flight Initiative," In: *Proceedings of IEEE Aerospace Conference 2016*. 5-12 Mar. 2016; Big Sky, MT.

[3]Chan, J., Wood, J.G., and Schreiber, J.G., "Development of Advanced Stirling Radioisotope Generator for Space Exploration," *proceedings of Space Technology and Applications International Forum (STAIF-2007)*, edited by M.S. El-Genk, AIP Conference Proceedings, 880, pp. 615-623, 2007.

[4]Wilson, S.D., Wong W.A., "NASA Glenn Research Center Support of the Advanced Stirling Radioisotope Generator Project," *NASA/TM-2015-218462*, NASA Glenn Research Center. April 1, 2015.

[5]Wong, W.A., Wilson, S.D., Collins J., and Wilson, K., "Advanced Stirling Convertor (ASC) Technology Maturation, *NASA/TM-2016-218908*. NASA Glenn Research Center. August 2016.

[6]Shin, E.E., "Evaluation and Validation of Organic Materials for Advanced Stirling Convertors (ASCs): Overview." In: *13th International Energy Conversion Engineering Conference (IECEC) Proceedings*. AIAA Propulsion and Energy Forum and Exposition 2015, ECD-02, Stirling Components session, 27-29 July 2015, Orlando, Florida.

[7]Shin, E. E., Sutter J. K., Thieme L., "Organics Evaluated for Advanced Stirling Convertor (ASC)," *R&T Research and Technology 2006*, NASA/TM 2007-214479, GRC, Cleveland, OH, p252-253, 2006.

[8]Shin, E. E., Scheiman D.,, Cybulski M.,, Quade D., Inghram L., and Burke C., "Validation of Organics for Advanced Stirling Convertor (ASC)," in *Proceedings of Space Technology and Application International Forum (STAIF)-2008*, Albuquerque, NM, Feb 10 – 14, 2008, AIP Conference Proceedings, Vol 969, Edited by M. S. El-Genk, pp 570-581.

[9]Mireles O. R., Shin, E. E., and Bowman C., Vesudevan L., "Mixed Neutron & Gamma-Ray Testing of Stirling-Alternator Candidate Organic Materials," *Proceedings of IECEC 2010*, 8th Annual International Energy Conversion Engineering Conference, Paper# 769917, 25 – 28 July 2010, Nashville, TN.

[10]Mireles O. R., Shin, E. E., and Bowman C., "Post-Irradiation Evaluation of the Stirling Alternator Radiation Test Article," *Proceedings of ICAPP 10*, San Diego, CA, USA, June 13-17, 2010, Paper 10008.

[11]Shin, E. E., Scheiman D.,, "Screening of High Temperature Organic Materials for Future Stirling Convertors," NASA/TM-2017, NASA Glenn Research Center. Submitted for publication, May 2017.